Insights into the interaction of a shale with CO2

Eleni Stavropoulou[1,*] and Lyesse Laloui[1]

[1]Ecole Polytechnique Fédérale de Lausanne (EPFL), Laboratory for Soil Mechanics (LMS), EPFL-ENAC-LMS, Station 18, CH-1015 Lausanne, Switzerland

[*]eleni.stavropoulou@epfl.ch

Abstract

Caprock formations such as shales, play a key role to safe underground CO_2 storage since they serve as a hydromechanical barrier that prevents migration of the injected CO_2 to the surface. While their hydromechanical response is important to ensure their sealing capacity, interaction with the injected CO_2 involves additional thermo-chemo-mechanical (THMC) phenomena that may threaten the long-term integrity of the caprock. The low transport properties of shales make them a suitable caprock material, but at the same time challenging to study due to the very long time scales (months/years) that are required for the various ~~thermo-hydro-chemo-mechanical~~ THMC processes to manifest. In this work, long-term the multiphysical interaction of the Opalinus Clay shale with liquid and supercritical CO_2 is studied in 3D with live x-ray tomography. ~~Long-term exposure to liquid and supercritical CO_2 targets the investigation of different occurring THMC processes in 3D.~~ 3D analysis reveals the localised response of the coupled THMC processes that is often indistinguishable with conventional lab testing protocols. To improve spatial and temporal resolution while applying ~~realistic~~ field-representative pressure and temperature conditions, small size samples are studied. Long-term injection of liquid CO_2 resulted in siginificant fissuring of calcite-rich zones that were for the first time visualised and quantified from the x-ray images. ~~, while~~ Additionally, a re-arrangement of the pre-existing micro-fissures in the clay matrix was observed. The volumetric response during direct exposure of an Opalinus Clay sample to supercritical CO_2 revealed an initial swelling at pre-~~cracked~~fissured zones and initiation of new micro-fissures at areas of direct contact with the anhydrous CO_2 due to pore water evaporation. Advanced 3D image analysis showed an increasing CO_2 uptake in the caprock material with time, ~~the elevated value of which after pressure release suggests~~ suggesting potential CO_2 trapping in the material.

1 Introduction

Geological CO_2 Storage (GCS) is an efficient way to permanently store large volumes of captured CO_2, by subsurface injection at pressures higher than its critical ~~phase point~~ pressure ($P_{cr,\,CO2}$ = 7.4 MPa) where it changes from gaseous to liquid state, and above a certain temperature level ($T_{cr,\,CO2}$ = 31.2°C) to supercritical. This ~~relatively~~ high pressure level strongly encourages the selection of deep reservoirs (min. 700-800 m depth), where the in situ water/brine pressure equilibrates the injected CO_2 pressure. According to the most recent IPCC report (IPCC, 2022), Carbon Capture and Storage (CCS) is key to reaching net-zero emissions by mid-century and mitigating climate change. Besides, the need to implement CCS in a range of sectors including energy production, manufacturing and industry is underlined in the same report.

The feasibility of the technology relies on successful long-term subsurface storage which depends – at least during the first few decades – on the performance of nearly impermeable geological formations (seal/caprock) that will prevent CO_2 migration to the surface. Caprock formations, typically shales or other tight mudrocks, are highly heterogeneous in mineralogy with low mass transfer properties and high sealing capacity.~~, and their prone~~ However, their response to Thermo-Hydro-Chemo-Mechanical (THMC) loads remains a complex subject that deserves further inquiry.

Shales have been studied since decades by the oil and gas industry, more recently for their use as geological barriers for ~~nuclear~~ radioactive waste storage, but full understanding of their suitability for geological CO_2 storage is still somewhat limited, since CO_2 injection further ~~complexifies~~ complicates an already difficult engineering problem: (i) Unlike ~~oil or~~ water or brine, CO_2 diffusion results in acidification of the in situ brine that can lead to chemical interactions in the caprock and alteration of its mechanical and transport properties (Yang et al., 2022); (ii) CO_2 injection introduces stress state changes in both the reservoir and the overlaying caprock that can cause reactivation of pre-existing faults or creation of new fracture systems (Vilarrasa et al., 2019).

Significant progress ~~in~~ on experimental data collection has been achieved ~~in~~ on various scales (Armitage et al., 2010; Houben et al., 2013), related to both geomechanical response (Rutqvist, 2012; Wang and Tokunaga, 2015; Kivi et al., 2022) and chemical interactions (Wollenweber et al., 2010; Hadian and Rezaee, 2020) during exposure to CO_2-rich fluids. Shales are anisotropic in their THM response and highly heterogeneous in mineralogy at different scales (micro to macro). ~~with~~ In particular, the strong geomechanical and geochemical couplings of shales ~~that~~ often challenge our ability to distinguish the different occurring phenomena and estimate their time-scale during CO_2 exposure.

In recent years, the Opalinus Clay shale has been studied as a potential caprock in the context of geological CO_2 storage (Amann et al., 2013; Favero et al., 2016; Makhnenko et al., 2017; Sciandra et al., 2021), ~~thanks to~~ because of its favourable properties, such as low porosity (< 20 %), low permeability (in the order of 10^{-20} m^2), high clay content (40-80 %), swelling properties and high sealing capacity (Marschall et al., 2005; Crisci et al., 2019; Delage and Belmokhtar, 2022). These favourable properties of Opalinus Clay (and shales more generally) make it a challenging material to study due to the slow flow processes at resolutions that may fall within the measurement error (Minardi et al., 2021).

Representative testing of shales remains a big issue. Testing conditions ~~Representative boundaries~~ do not only involve the applied level of pressure or temperature but also the spatial and temporal scale of the measurement. ~~While~~ Whereas large scale experiments are generally considered to be more realistic, they can be challenging to properly monitor and analyse since they involve the combination of multiple phenomena ~~occurring~~ that occur under different scales, in particular in heterogeneous materials such as shales. A real scale experimental campaign has been recently completed at the Underground Research Laboratory (URL) in Mont Terri, where CO_2-rich brine has been injected in an existing fault in Opalinus Clay (Zappone et al., 2021). The results have not been conclusive, ~~given~~ mainly due to the low applied pressure, the small volume of injected CO_2 and the long time-duration that is required for transport phenomena to manifest ~~in~~ on that scale. In parallel, recent lab-scale experimental results from CO_2 injection tests in Opalinus Clay samples, do not show evidence of significant influence on the ~~material's basic~~ fundamental properties of the material for the given test duration ~~(Minardi et al., 2021; Favero & Laloui, 2018);~~: grain density, dominant entrance pore size and void ratio, as well as hydraulic conductivity do not vary in a considerable way after exposure to

CO_2 over a ~~weekly~~ time-scale of a few weeks (Minardi et al., 2021; Favero & Laloui, 2018). The short duration of these tests together with the ~~chosen~~ sample size could be among the reasons for the absence of measurable evolution.

Representative testing conditions and duration are even more challenging when processes of geochemical nature are investigated. ~~Indeed, the impact of chemical reactivity of shales in the presence of CO_2 remains a very challenging topic.~~ While shales contain minerals reactive to CO_2, current lab measurements are not ~~enough~~ sufficient in identifying chemical interactions directly, since they rely either on post-mortem analysis of fluid composition or mineralogy (Armitage et al., 2013; Elkady and Kovscek, 2020). The indirect interpretation of permeability results before and after CO_2 exposure ~~in terms of chemical alterations (dissolution/precipitation)~~ can be ambiguous in terms of chemical alterations. ~~since~~ This is because they may involve self-compensating mechanisms such as carbonate dissolution, mechanical crushing and inelastic compaction, as shown by various authors who studied fractured caprock samples (Yasuhara et al., 2011; Hashemi and Zoback, 2021). It is thus difficult to build solid conclusions on the impact of chemical interactions on the structural properties of the material, and consequently on its transport and mechanical response.

Taking all the above into account, there is a series of issues when testing shales in the context of CO_2 storage: (i) Flow is extremely slow, resulting in long testing durations; (ii) Measured permeability variations are close to the measurement error; (iii) Reproduction of real site conditions is crucial since injection pressure, and therefore effective stress, has an important impact on properties of the material that drive flow and breakthrough, i.e. connected porosity; (iv) Chemical interactions are limited by the slow transport properties of the material; (v) The testing duration ~~and scale that are commonly used are~~ is usually not enough to allow investigation in that direction.

In this work, the different coupled processes and phenomena that occur when CO_2 interacts with a shaly caprock material – the Opalinus Clay – are explored based on a series of measurements and observations from real time x-ray tomography. Taking full advantage of this non-destructive tool, new aspects and results are targeted ~~and demonstrated that aim to~~ aiming at improving ~~improve~~ our understanding of the caprock~~'s~~ response ~~while~~ under field-realistic testing conditions. The originality of the presented research relies mainly on two aspects: first, ~~on~~ the study of smaller size samples, where observation period is expected to be shorter, and second, ~~and most importantly~~ on the direct measurement of strain fields and structural alteration from the 3D analysis of the ~~3D~~ tomographic images. In the following, the proposed methodology, tools and conventions of analysis ~~conventions~~ are presented in detail. The results of two experimental campaigns where Opalinus Clay ~~shale~~ is exposed to either liquid or supercritical CO_2 are presented and discussed. These experiments target different coupled mechanisms, that combined, aim to contribute to a more profound understanding of the overall THMC response of shales with CO_2.

2 Methodology, tools and principles of analysis

Shales are highly heterogeneous and anisotropic materials, sensitive to ~~thermo-hydro-mechanical~~ THM variations, ~~and~~ with strong multiphysical couplings and very slow transport properties (Mohajerani et al., 2014; Favero et al., 2016; Menaceur et al., 2016; Li and Laloui, 2017). Inevitably, representative testing of shales requires the employment of methods and tools that can embrace these particularities. These should include ~~by means of~~ controlled applied conditions and full-field measurement, i.e. a field record of a quantity (e.g., deformation, density, temperature, etc.) as opposed to point-wise data (Viggiani and Hall, 2008).

Taking into account all the above, the ~~exploration~~ development of a new approach in testing shales with in situ x-ray tomography is motivated. In this study, the full-field of micro-structural variations and kinematics of the Opalinus Clay shale when exposed to CO_2 under different boundary conditions are targeted with 3D image analysis of real-time x-ray tomographies. Long-duration exposure of Opalinus Clay to injected liquid CO_2 (8 MPa) under confined conditions (10 MPa) aims to reveal potential chemo-mechanical processes.~~, while d~~ Direct exposure of unjacketed Opalinus Clay to supercritical CO_2 targets the better understanding of localised THM interactions that are otherwise difficult to detect with conventional lab-testing techniques.

Despite the classic testing approaches on centimetric size shale samples in the literature, in this work ~~very small~~ micro-samples (5 mm) are studied in order to first, ~~gain in~~ improve the temporal resolution (partly inspired by small-scale permeability testing equipment (Birmpilis et al., 2019; Birmpilis and Dijkstra, 2021), but also to optimise the quality of x-ray imaging (improved spatial resolution). This approach is challenging for the given material and the given subject. ~~; t~~ The pore size of shales is in the order of nanometres and thus impossible to visualise with x-ray micro-tomography (micrometric scale). Nonetheless, observation and quantification of microstructural modifications due to interaction with CO_2 can be explored with ~~relatively~~ high scanning resolutions (5-8 μm/px) and fast tomographies thanks to the small size of the sample.

2.1 In situ x-ray micro-tomography and experimental protocol

A few authors have investigated the mineralogical heterogeneity and THM anisotropic behaviour of shales, pointing out the role of the microstructure ~~by employing~~ with the employment of different imaging techniques (Wang et al., 2013; Desbois et al., 2017; Delage & Tessier, 2021). In the case of experimental geomechanics, x-ray tomography is the most widely used technique, with a large range of results stated in literature (Viggiani et al., 2015; Bedford et al., 2017; Vego et al., 2022; Birmpilis et al., 2022). The great advantage of x-ray tomography compared to other techniques for soil characterisation (e.g. SEM microscopy), is the possibility to identify ~~in 3D the specimen's heterogeneity~~ the mineralogical heterogeneity of the specimen in 3D and follow its evolution in time (in situ testing). ~~This~~ X-ray tomography is a very powerful tool that allows a better interpretation of test results, such as measured permeability, ~~fingering phenomena~~ fissuring, localised deformation or structural modifications (Voltolini and Ajo-Franklin, 2020; Stavropoulou et al., 2020).

For this study, the dual x-ray source in PIXE platform for x-ray micro-tomography (EPFL, Switzerland) is used. Reconstructions are performed with the XAct software provided by RX-Solutions (Annecy, France), with appropriate beam-hardening corrections applied. A cylindrical cell made out of PEEK (polyether ether ketone) is used for the application of the various boundary conditions, that are explained in detail in the following sections. The so called PEEKcell is fixed on the rotating table, as close as possible to the x-ray source, for a maximal use of the x-ray conical beam. All scans are performed in temperature controlled environment ~~of~~ at 21°C. ~~A cylindrical cell made out of PEEK is used for the application of the various boundary conditions, that are explained in detail in the following sections. The so called 'PEEKcell',~~ The PEEKcell is designed to host 5 mm × 5 mm cylindrical samples and can sustain a maximal pressure and temperature of 20 MPa and 80°C respectively (Stavropoulou and Laloui, 2022). An entry on each side of the cell (top and bottom) allows the application of confining pressure (top) and pore pressure (bottom) on the sample. The cell is disconnected from the pressure controllers and transported under the ~~given~~ pressure state in the tomograph.

To monitor the pressure level during the scans, a pressure transducer is placed on ~~each side~~ both ends (see Fig. 1).

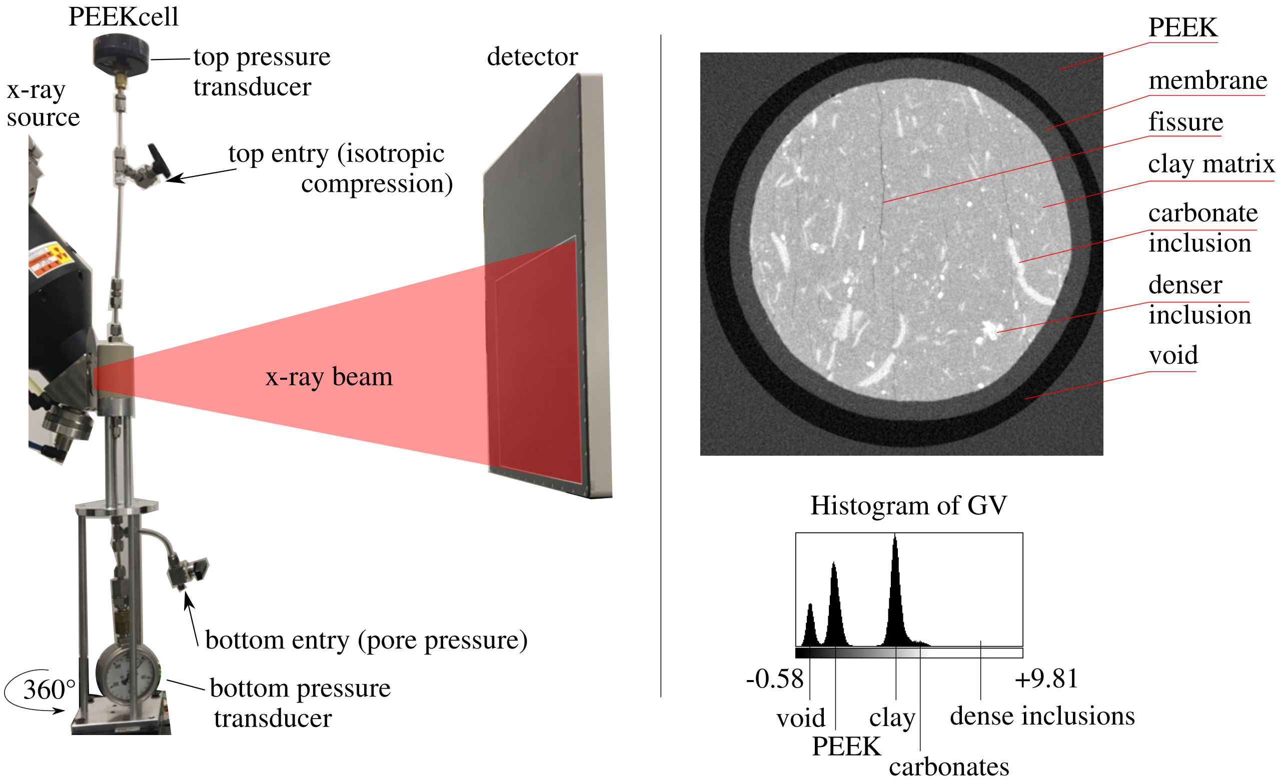

Figure 1: (left:) PEEKcell setup in the x-ray tomograph, (right:) horizontal slice of a reconstructed x-ray image and the corresponding histogram of ~~greyvalues~~ grey values

The samples are cut to cylindrical shape of d = h = 5 mm~~; first sized down in~~ by cutting rectangular pieces with a saw, ~~and~~ which were then reduced to the desired size manually using fine sand paper (P240). This technique has been preferred (to a mechanical lathe for example) in order to avoid overheating the sample during preparation. The resaturation of the samples has been achieved progressively under free swelling conditions by exposing the samples in a ~~controlled~~ relative humidity (RH) controlled environment with the use of an appropriate saline solution (Romero, 2001)~~;~~: first to RH = 75 % (NaCl) and then RH = 98 % (K_2SO_4) until mass stabilisation. Before testing, samples have achieved a close-to-full saturation state, corresponding to a measured water content w_{resat} = 6.1 - 6.8 %, i.e. within the range of full saturation (Bossart and Thury, 2011).

In this work, first the micro-structural modifications due to long-duration CO_2 exposure are investigated with post-mortem measurements and analysis, i.e. after removing the applied pressures. Then, the occurring kinematics on Opalinus Clay that is exposed in direct contact (no sealing membrane) with supercritical CO_2 ~~is~~ are examined with in situ measurements, i.e. while under pressure in the cell. According to the volumetric response of the sample and the corresponding grey values (GV) of the x-ray images, the CO_2 uptake is investigated and visualised. ~~for the first time.~~

When supercritical CO_2 is injected, a thermal jacket is used around the cell and the applied temperature is monitored with a thermal sensor that is placed between the jacket and the PEEKcell. For achieving a maximal resolution and x-rays penetration the thermal jacket is removed during the scans. Inevitably, this leads to CO_2 phase change from supercritical (lower density) to liquid (higher density) and consequently to a pressure drop under constant volume conditions, i.e. conditions during scanning. ~~In order to minimise this pressure drop, t~~ The cell is exposed to the ~~scanner's~~ temperature of the scanner (21°C) two hours in advance, while maintaining the pressure at the desired level (pressure pump connected), in order to avoid pressure loss due to phase change during the scan. The possible implications of this CO_2 phase transition before the scans ~~on the given testing campaign~~ are discussed in the corresponding section of direct exposure to supercritical CO_2.

2.2 Image analysis

The result of an x-ray tomography is a 3D x-ray attenuation map of the scanned sample that is associated to the 3D density map of the material. For instance dense phases in the material (non-clay mineral inclusions) attenuate more x-rays than lower density phases (e.g. cracks, pores). The different density (attenuation) levels ~~reflect~~ are reflected in the grey level values ~~(GV)~~ of the reconstructed 3D x-ray image.~~; h~~ Higher GV corresponds to denser phases and lower GV to ~~lower~~ less dense phases as indicated in Fig. 1-right. Changes in the GV of a ~~scanned~~ sample image in time or due to application of a different load, allow the observation and quantification of localised micro-structural modifications (e.g. crack opening/closing, swelling/shrinking) which can subsequently be translated to 3D strain fields with Digital Volume Correlation (DVC). In this work, the open source SPAM software (Stamati et al., 2020) is used for the DVC analysis.

In DVC, two images are required~~;~~, an initial (reference image) and a deformed one. In the case of local-DVC (that is used for the image analysis in this work), a grid with a given node spacing is defined and at each grid point a centred window is extracted. For each of these subvolumes a linear deformation function Φ is calculated so that $\text{image}_{\text{deformed}}\ (\Phi\cdot \text{x}) = \text{image}_{\text{reference}}(\text{x})$. The function Φ

accounts for translation, rotation and stretching and its calculation is optimised by solving an iterative problem that minimises error based on the classic sum of squared difference (SSQD). ~~While~~ Whereas DVC can calculate a strain field ~~and~~ that can then be applied ~~it~~ on an image, it does not take into account by definition the variations of ~~the~~ GV due to the corresponding strain. Deformation-based GV correction ~~due to deformation~~ as per Stavropoulou et al., (2020) is going to be applied in this work, ~~as per (Stavropoulou et al., 2020) where the aim is~~ aiming to investigate phase changes due to chemical reactions between the in-contact CO_2 with the same material.

~~All scans of each type of test~~ For each type of test, all scans are performed under the same conditions and with the same scanning parameters. Nevertheless, noise, artefacts or other external changes may be present between the different scans ~~(that in some cases are performed in month intervals)~~. To improve the accuracy of image analysis and minimise the GV variations due to measurement conditions rather than real changes in the material, all images from ~~a~~ the same testing campaign are normalised based on GV of materials, the density of which is not supposed to vary between the different scans~~;~~ (here PEEK and aluminium). ~~The procedure of the GVs~~ GV normalisation ~~is explained in detail in the Appendix and~~ results in scaling the given images so that the voxels that correspond to void are set to GV = 0 and those of PEEK correspond to GV = 1. The followed procedure is explained in detail in the Appendix.

Finally, ~~for the strain field calculation,~~ the occasional rigid-body transformation of the sample (translation and rotation) ~~due to transportation and re-installation of the cell in the tomograph,~~ is calculated based on ~~the~~ a single Φ function ~~on~~ for the entire image (so called registration) and removed. DVC is then performed between the reference image and the deformed ones, from which rigid body motion has been corrected. The displacement field is then calculated and ~~translated~~ converted to strain assuming small transformations (see details in Stamati et al., 2020). The above principles and conventions are applied for the analysis of the different series of x-ray scans that are presented in the following.

Correction of x-ray attenuation due to volumetric strain

Taking into account the measured strain field from the DVC analysis, the variation of the x-ray attenuation coefficient (μ_x) in time is corrected and measured. Volumetric strain results in density variation (and therefore μ_x variation) that is manifested in the GVs level of the deformed image via a linear relationship. A simple example to better understand this reasoning is the case of thermal expansion with no mass transfer, where the density of the material is expected to reduce, and consequently the attenuation field μ_x or GVs to decrease proportionally to the change in density. Any additional GV variation is therefore assumed to be due to additional mass transfer (gain or loss), which in this workis due to CO_2 uptake. After Stavropoulou et al., (2020), the attenuation variation $\Delta\mu$ of a sample is calculated as a function of the mechanical volumetric strain assuming mass conservation:

$$\Delta\mu = -\varepsilon_v \cdot \mu_0 \tag{1}$$

where ε_v is the measured volumetric strain of the sample and μ_0 is the initial attenuation of the image (before loading).

In order to measure the additional changes of GVs due to mass transfer, the calculated strain field is applied on the reference image (e.g. scan 00), while taking into account the corresponding GV correction. Then, simple subtraction of the deformed image (with corrected GVs due to volumetric variation) from the corresponding original image (e.g. 01 minus 00_def_to_01) results in the uptake or loss of mass.

3 Long-term micro-structural modifications

In this section, the long-term chemo-mechanical interactions that can occur between CO_2 and a shaly caprock are explored. ~~Taking into account the small size of the samples (5 mm × 5 mm), first~~ First, a mineralogical analysis of different Opalinus Clay samples is performed with x-ray diffraction (XRD) measurements, in order to evaluate the mineralogical variability given the small size of the samples (5 mm × 5 mm). Then the mineralogical map of an Opalinus Clay sample is studied with SEM-EDX (scanning electron microscopy and energy dispersive x-ray) measurements and the identified mineral locations ~~is~~ are directly compared and identified in the corresponding slices from the x-ray tomography image of the same sample. The goal of this combined analysis is twofold. ~~This combined analysis~~ On one hand, it aims ~~to locate~~ at locating and ~~demonstrate~~ showing the presence of elements in the sample that may favour chemical interactions in the long-term presence of CO_2 (e.g. Ca, C, Si, S, O etc.). ~~that is here investigated with x-ray tomography by means of, and~~ On the other hand, this analysis aims at evaluating the response of the identified mineral phases based on the occurring micro-structural modifications that are identified from x-ray tomography (fissuring, swelling, self-sealing etc.).

Table 1 shows the mineralogical composition of four sister Opalinus Clay samples (shaly facies) from XRD measurements. The fit was optimised on one sample and to increase comparability, the next fits were done by keeping all refined parameters and replacing the data file on the current model. ~~Even though the results are quite approximate, a~~ A similar quartz and clay content is measured for all samples except for illite that presents variations up to 8 %. In the lower illite-rich samples a higher calcite content is measured with values that vary among the different samples from 13 % to 24 %. The different content values that are presented for sample A (in bold), are measured after long-term exposure to CO_2. ~~The mineral content of sample A (in bold) is measured after long-term exposure to CO_2.~~ It presents a high ~~clay~~ calcite content that is unclear if it is affected in any way by its previous interaction with CO_2 since its overall mineral content falls within the variability of the other three untreated samples. ~~Even~~ Nevertheless, even after long-term CO_2 exposure, ~~its~~ the mineralogical composition of sample A does not vary in a significant way compared to the other three untreated samples. Sample A is used to compare the results from all different ~~analysis~~ imaging tools that are employed for this study.

Opalinus Clay (wt %)	**A**	X	Y	Z
Calcite	**21**	13	16	24
Quartz	**13**	13	14	11
Chlorite	**15**	15	13	17
Kaolinite	**3**	2	2.5	1.5
Illite	**45.5**	53.5	52	45.5
Siderite	**2**	2	2	11.5
Pyrite	**0.5**	0.5	0.5	0.5

Table 1: Mineralogical composition of four sister Opalinus Clay samples based on x-ray diffraction

The mineralogical nature of the non-clay inclusion phases of the x-ray tomography images are identified with SEM-EDX measurements. ~~In order to confirm the mineralogy of the inclusions identified from x-ray tomography, sample A has been subjected to a SEM-EDX analysis.~~ The height of the sample is carefully reduced to the height of the horizontal slice of Fig. 2 (a) using ~~again light~~ sandpaper (the traces of which are apparent in the SEM images). Figure 2 presents the combined information obtained ~~both from~~ from both x-ray tomography and SEM-EDX at the same horizontal slice. In Fig. 2 (a) ~~the x-ray slice~~, the different GV levels of the x-ray slice highlight the distribution of the different inclusions in the clay matrix, the mineralogy of which is identified from the EDX analysis. ~~In fact, t~~There are two sets of inclusions as revealed from the GV histrogram plotted in Fig. 2 (b). ~~This is more clear when a bilateral filter is applied (red histogram) that unveals a second peak that represents the lower GV inclusions.~~ This becomes more significant by taking into account that a second peak representing the lower GB inclusions is visible after the applications of a bilateral filter.

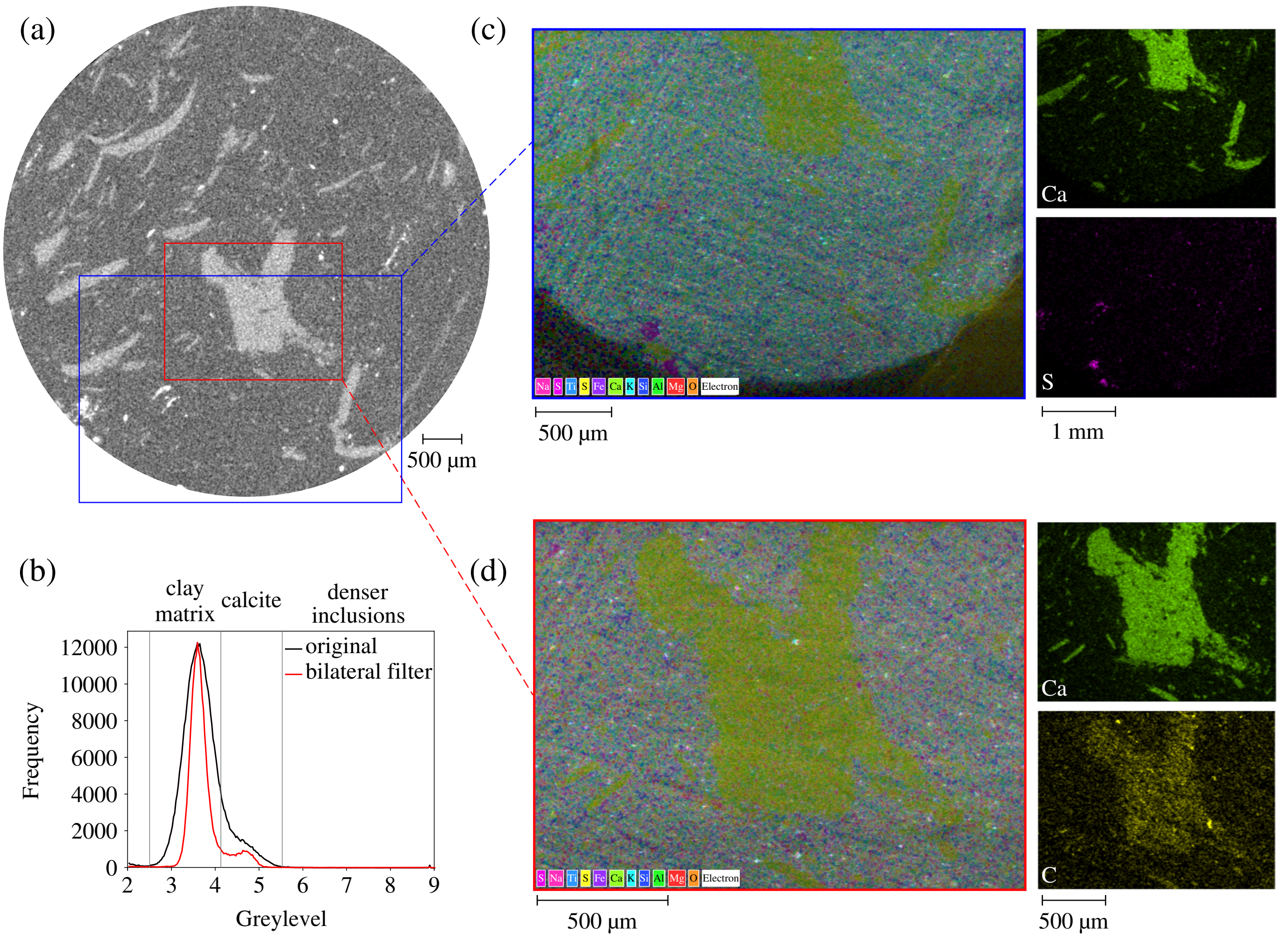

Figure 2: Identification of the inclusions mineralogy combining x-ray tomography and SEM-EDX – (a) horizontal x-ray tomography slice, (b) histogram of GVs of the top horizontal slice, (c) SEM-EDX map corresponding to the blue window of the x-ray slice highlighting all identified elements and the areas rich in Ca and S, (d) SEM-EDX map corresponding to the red window of the x-ray slice highlighting all identified elements and the areas rich in Ca and C

These lower GV level inclusions are rich in calcium (Ca) and carbon (C), i.e. calcite ($CaCO_3$), as revealed from the EDX images (Fig. 2 (a) and (d)). ~~This type of~~ These carbonate inclusions are therefore ~~more~~ prone to ~~undergo dissolution~~ react (dissolve) in the presence of CO_2. The denser inclusions (~~whiter~~ brighter inclusions in Fig. 2 (a) at the bottom left of the sample) seem to be rich in sulphur (S) (see Fig. 2 (c)), a main element of pyrite (FeS_2) the density of which is very high. ~~This supplementary EDX measurement reveals that the information from the 3D x-ray images is even richer than what has widely been used for now.~~

Sample A is the same sample that has been used in (Stavropoulou and Laloui, 2022).~~; i~~ It has first been scanned in the x-ray tomograph under unconfined conditions, then after application of confinement (10 MPa) ~~followed by CO_2 injection~~ CO_2 was injected up to a pressure of 8 MPa (pixel size 7.8 μm). After CO_2 breakthrough, it has been ~~let~~ held under constant volume conditions in the PEEKcell for 9 months and scanned again in the x-ray tomograph after pressure release (same pixel size and scanning parameters). It is important to mention that there has been pressure loss during these 9 months that has not been properly monitored: during the last 5 months the confining pressure has been reduced to half and the CO_2 pressure to 1 MPa. Nevertheless, the results present great interest and possible impact of this pressure loss is discussed in Section 5. ~~that is not necessarily impacted by this pressure loss.~~

Figure 3, shows a horizontal and vertical slice of two x-ray scans of sample A, initially and after 9 months of CO_2 exposure, both in unconfined conditions. ~~The micro-fissures have been manually highlighted in black for more clarity, but the entire volumes can be found at their original form in the supplementary material. The initial image of the sample reveals a vertical bedding orientation according to the orientation of the pre-existing fissures in the clay matrix.~~ In its initial state, the sample contains a series of pre-existing fissures in the clay matrix of vertical orientation, i.e. similar to the bedding orientation. After 9 months of CO_2 exposure there are two important observations to be pointed out. First, clear fissures in the carbonate phases have been formed ~~revealing the~~ suggesting calcite dissolution for the first time from x-ray images ~~and~~ under ~~non-extreme (if not realistic) testing~~ realistic pressure and temperature conditions. In addition to the fissuring of the carbonate inclusions, a disappearance of the initially pre-existing fissures in the clay matrix is observed. ~~This can be explained first, by means of self-sealing behaviour of the material under long-duration application of confinement. Another possible mechanism could be related to precipitation of Si-rich zones that are not distinguishable from the x-ray images, since they have similar density with the clay minerals.~~

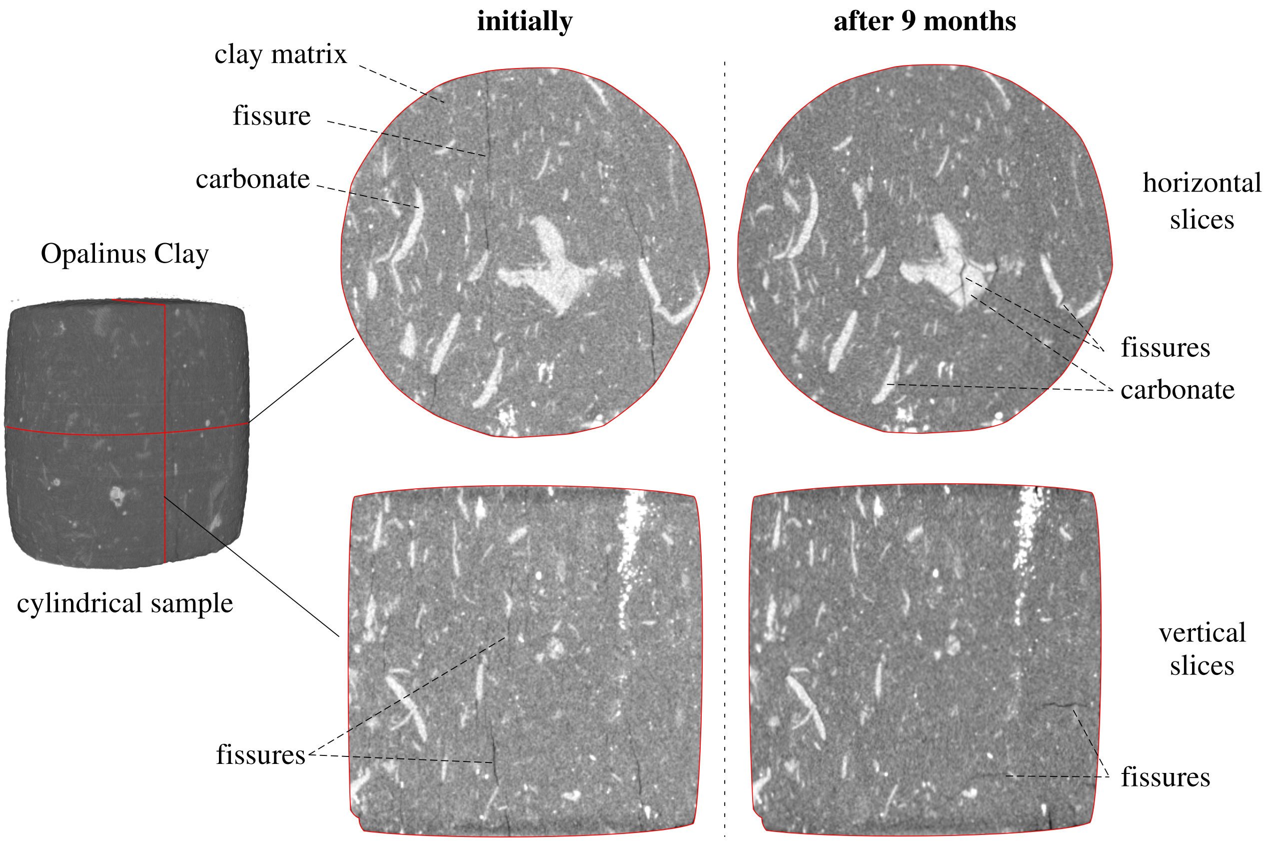

Figure 3: Horizontal and vertical slices of x-ray tomography on the same Opalinus Clay sample with highlighted fissures (in black) under unconfined conditions at its initial state (left) and after 9 months CO_2 exposure (right). The horizontal slices (top) highlight the fissuring of the carbonate phase due to dissolution and the self-sealing of the clay matrix pre-existing fissures under long-term confinement; the vertical slices (bottom) highlight the fissure rearrangement and change of orientation that took place in time.

~~Prakash et al., (2022) pointed out a more pronounced precipitation activity in zones parallel to the direction of the bedding plane. Self-sealing and precipitation are two phenomena independent from each other and they can occur at different time-scales.~~

For a better understanding of the micro-structural modification of the sample after long-term CO_2 exposure, the orientation of the minimum eigenvectors of the moment of inertia is calculated for each identified inclusion and micro-fissure. This corresponds to the ~~(~~longest axis~~)~~ of ~~the inclusions and micro-fissures~~ each labeled inclusion or micro-fissure. ~~have been plotted in~~ The 3D orientations together with their projection in the 2D plane~~, as shown~~ are plotted in Fig. 4. Both types of orientation plots are presented for a better demonstration of the result of each studied phase.~~—t~~ The 3D histogram is more comprehensible for the ~~cracks'~~ orientation of the cracks and the 2D projection for the inclusions. For this analysis, a bilateral filter has been applied on the two images to reduce noise and to smoothen the edges between the different phases (clay/cracks, clay/inclusions). In this way a better segmentation of the phases of interest (cracks and inclusions) can be achieved.

~~Even though these results could be optimised from a quantitative point of view, the overall shape modification of the two segmented phases is realistic.~~

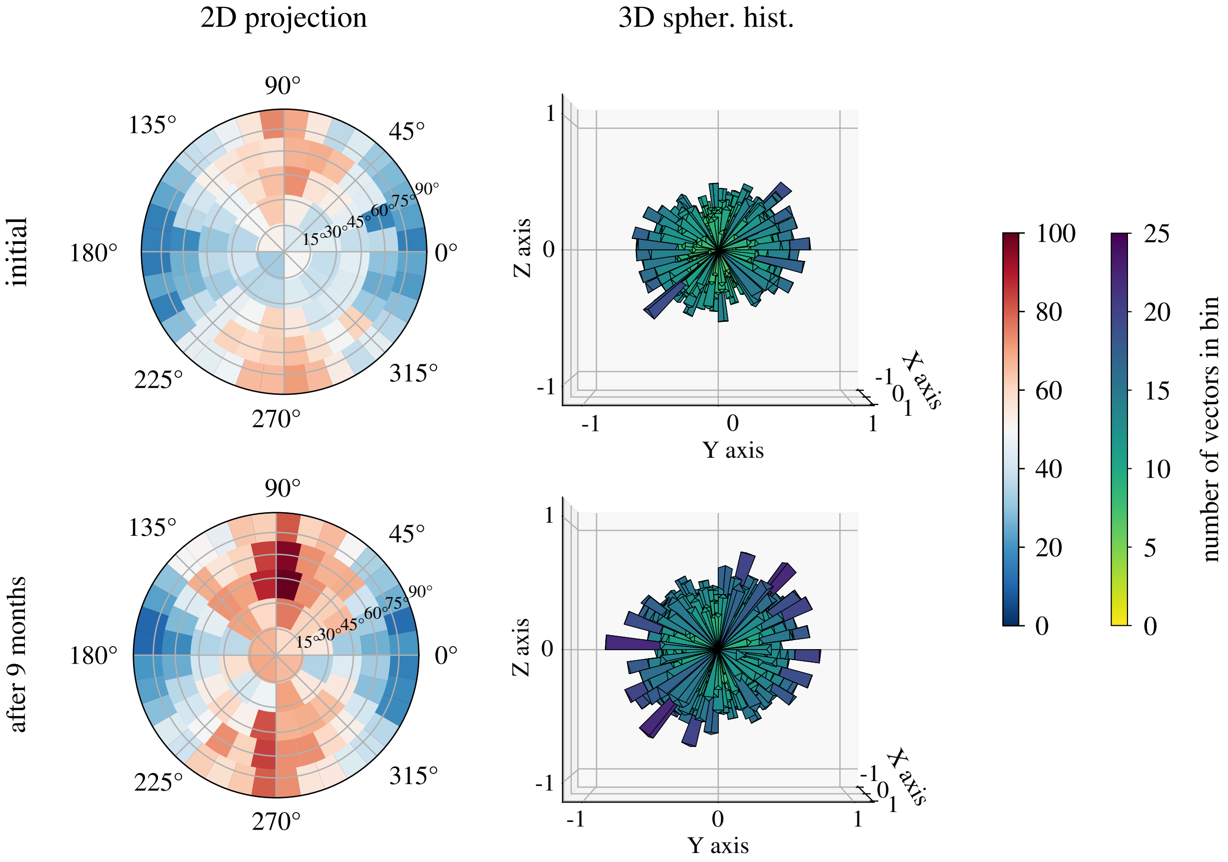

Figure 4: 2D projection (left) and spherical histogram (right) of the minimum eigenvectors of sample~~'s~~ 02 inclusions, initially and after 9 months exposure to CO_2

The 2D projection of the ~~min.~~ minimum eigevectors of the inclusions reveals a preferential orientation along the vertical axis – i.e. axis parallel to the bedding plane – both initially and after 9 months exposure (Fig. 4). The vertical axis of the 2D plots is parallel to the Y axis of the spherical histograms that are plotted in this view to demonstrate the ~~vectors'~~ orientation of the eigenvectors on the ZY plane. After 9 months exposure to CO_2 the population of inclusions is increased as demonstrated by both plots ~~on the right~~ at the bottom of Fig. 4. This increase in the number of inclusions is ~~a clear~~ considered as an indication of carbonate dissolution that resulted in inclusion fissuring and consequently identification of more numerous inclusion particles. The main orientation axis after dissolution remains vertical, suggesting that fissuring ~~due to dissolution~~ in the carbonate particles has mainly occurred along their shortest axis ~~of the inclusions~~ and therefore perpendicularly to the bedding plane.

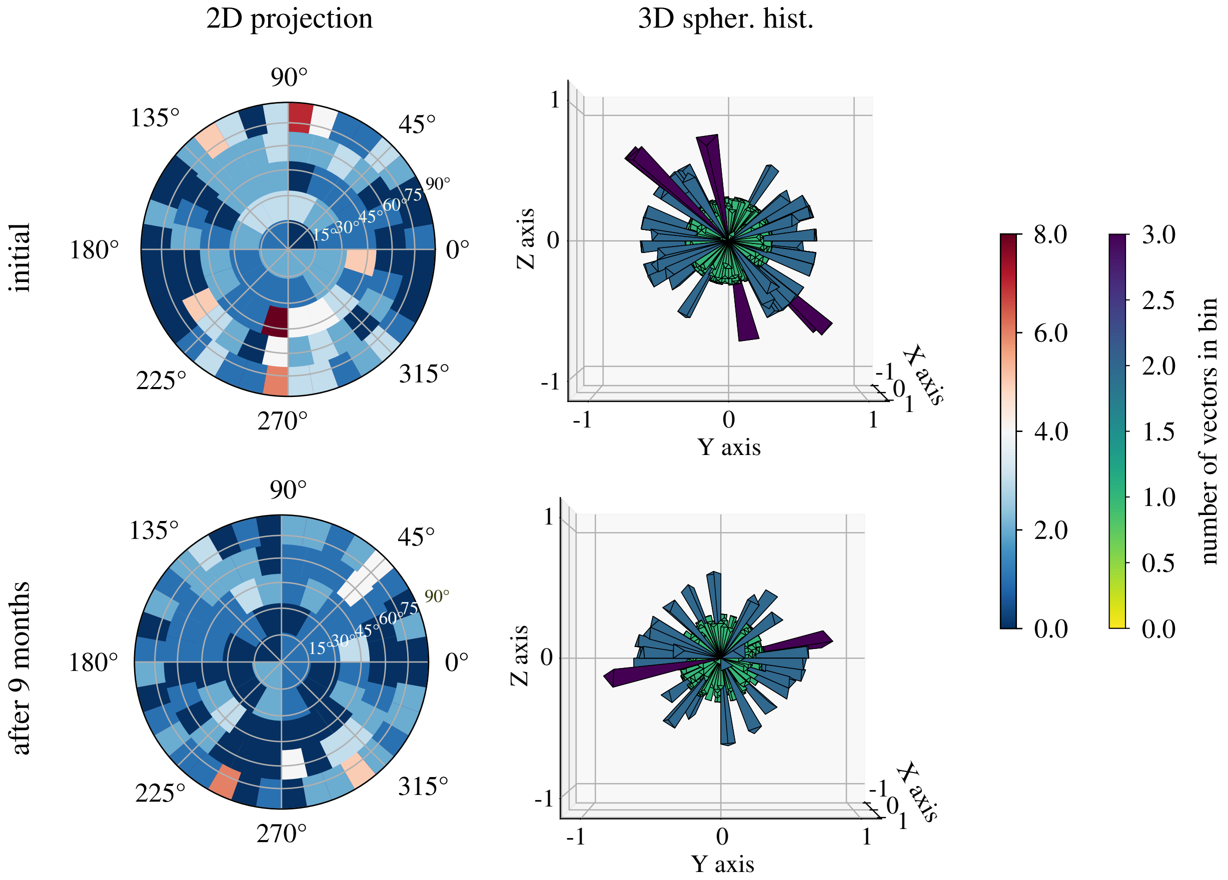

Figure 5: Spherical histogram of the minimum eigenvector of the inclusions and the cracks in sample A, initially and after 9 months exposure to CO_2 (colour represents the number of projected points per bin divided by the median number of points in all bins)

In a similar way, the 2D projection and the spherical histograms of the minimum eigenvector of the ~~sample's~~ identified cracks in the sample ~~and their 2D projection~~ are plotted in Fig. 5~~;~~: initially and after 9 months of CO_2 exposure. The initial shape of the 3D histogram ~~initially~~ reveals the preferential orientation of the micro-fissures parallel to the bedding plane. ~~sample's anisotropy with a preferential orientation parallel to the bedding plane.~~ This is confirmed by the high number of vectors projected on the vertical axis of the 2D plot. ~~— even though the low number of cracks make it harder to evaluate. Interestingly, the shape of the 3D crack histogram on the right is very different, confirming the observations and assumptions discussed from Fig.~~ 3. After 9 months of CO_2 exposure, the shape of the 3D crack histogram is modified. ~~First,~~ On one hand, the number of cracks is reduced, ~~validating the self-sealing (or precipitation) response of the sample after long-duration confinement. most importantly,~~

and on the other hand, the orientation of the main pre-existing cracks ~~has been totally modified and is no more~~ is no longer parallel to the bedding. ~~It is not clear whether these new fissures are the result of alteration of the pore fluid's pH that enhances further chemical reactions between minerals that are not detectable from x-rays and CO_2, or whether they are related to mechanical impact from CO_2 breakthrough (see 3D volumetric response after breakthrough in Stavropoulou and Laloui, 2022). In either case, this result points out a potential rearrangement of the fissure network after long-term CO_2 exposure that has not been previously discussed. Most importantly, these results show how little we still know regarding the coupled long-term THMC response of the caprock/CO_2 interaction at the micro-scale and their implications to the large scale response. Longer-duration testing under realistic boundary conditions are required for a better understanding of the complex mechanisms that occur.~~

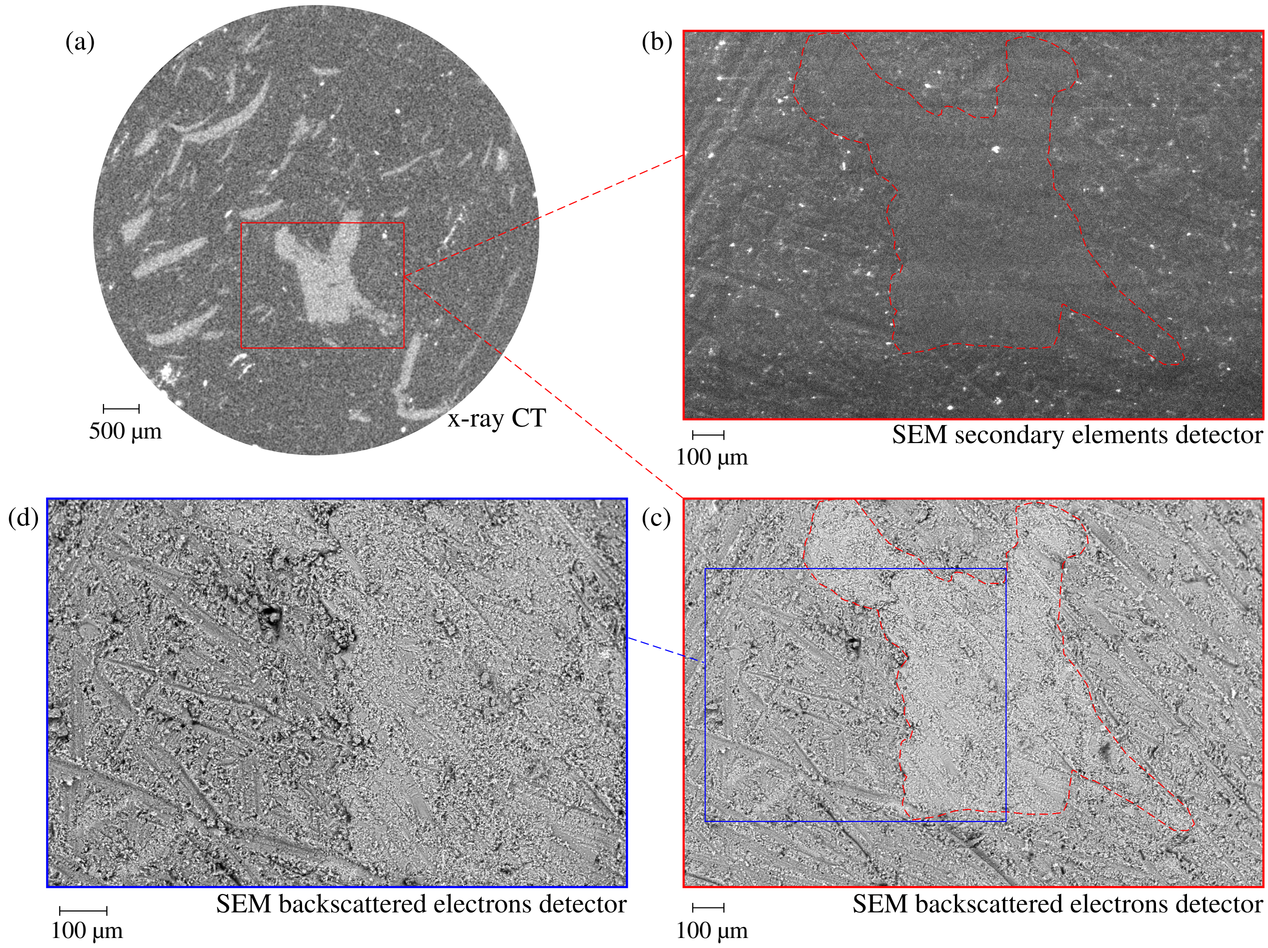

Figure 6: Horizontal slice of the Opalinus Clay sample A from different imaging tools, (a) x-ray computed tomography, (b) corresponding SEM slice scanned with a secondary elements detector, (c) corresponding SEM slice scanned with a backscattered electrons detector, (d) magnified selected region of (c)

Finally, in the aim of a better visualisation of the texture of the carbonic inclusions, the SEM image of the same (unpolished) slice with Fig. 2 is presented in Fig. 6. For the SEM images, two detectors have been used~~;~~: (top) a secondary elements detector that basically illustrates the surface topography~~;~~, and (bottom) a backscattered electrons detector that shows a Z contrast, i.e. lighter elements (such as Si, Al, O, K) are darker and heavier elements (here Ca or C) are brighter. The secondary elements detector does not reveal any information regarding the targeted inclusion other than the fewer sandpaper traces that are ~~very~~ more obvious on the softer clay matrix. On the other hand, the backscattered electrons detector provides a better distinction between the two phases. The higher resolution of SEM allows a better visualisation and understanding of the interface between the carbonate inclusion and the clay matrix that is otherwise not visible ~~with x-rays~~ from the x-ray images. ~~While~~ Even though the resolution is still in the micrometric scale and no nanometric pores can be detected in either types of images, a distinct calcite/clay interface of increased porosity is revealed in the zoomed area of the bottom SEM image (blue window). These results confirm the findings of Minardi et al. (2021) on carbonate rich Opalinus Clay shale that identified a bimodal pore size distribution, with a second dominant pore size between 50-100 μm corresponding to the interface of carbonate/clay particles. ~~The high inter-particle porosity can serve as a preferential CO$_2$ pathway and eventually enhance geochemical interactions, in this case carbonate dissolution.~~

4 Direct exposure to supercritical CO2

In this part, the interaction of an Opalinus Clay sample with supercritical CO$_2$ is evaluated in time by means of quantitative 3D x-ray image analysis. The unjacketed (no membrane) caprock sample is exposed from all sides (equilaterally) to direct contact with supercritical CO$_2$ ~~(~~ at p = 10 MPa and T = 34°C~~)~~ pressure and temperature conditions respectively. ~~and regular x-ray scans (resolution 5.38 μm/px) are performed f~~ For the study of its volumetric and micro-structural response regular x-ray scans (resolution 5.38 μm/px) are performed. The water saturated sample is mounted in the PEEKcell and a first scan (00) is performed under ~~initial~~ ambient unconfined conditions. CO$_2$ is then introduced in the cell in direct contact with the sample. The target pressure and temperature are applied and maintained stable over a period of 56 days. ~~Then, the target pressure and temperature are applied and the sample is let to interact with the in-contact CO$_2$.~~ Further scans of the sample are performed while under pressure in the PEEKcell after 13 days (scan 01), 30 days (scan 02) and 56 days (scan 03) of CO_2 exposure. ~~, as well as~~ A final scan is performed after the release of pressure and temperature (scan 04 at 56 days).

4.1 Volumetric response

The 3D volumetric response of the caprock material under the above mentioned conditions ~~are~~ is evaluated and quantified by means of DVC analysis. As explained earlier, to properly compare and analyse the acquired images, the occasional rigid-body transformation (translation and rotation) is removed so that the images are well aligned, as shown in the left column of Fig. 7. The middle vertical slice of the tested sample reveals the pre-existence of 3 principal horizontal fissures parallel to each other and parallel to the bedding orientation of the sample, i.e. perpendicular to the vertical axis of the sample. These micro-fissures ~~of~~ with an initial ~~max.~~ maximum aperture of $\approx 30\ \mu$m may have been induced during sample preparation and/or during resaturation under free swelling conditions. Their existence is not necessarily an issue for the given study.~~; o~~ On the contrary they can provide important insight into the impact of their presence upon interaction with CO_2. For instance, an increasing opening of the bottom fissure can be observed in time, directly from the x-ray slices in Fig. 7 (left). Moreover, the creation and propagation of additional new micro-fissures at the bottom of the sample can be observed with time, as highlighted in the same slices. ~~Looking more closely at the microstructure of the middle slice in Fig.~~ 7 ~~an increase of the bottom principal pre-existing fissure can be observed, as well as the creation and propagation of additional new micro-fissures at the bottom of the sample; between the bottom left inclusion structure and the lower principal fissure.~~

For a more quantitative analysis of the localised response of the sample, the volumetric strain is calculated in 3D between each scan and the initial state of the sample (scan 00) that is used as reference. For the DVC analysis, the chosen parameters (half window size, node spacing etc.) are detailed with the additional provided data online. The map of the calculated volumetric strain of ~~each~~ the middle vertical scan slices is presented on the right column of Fig. 7. ~~where the corresponding middle vertical slice is shown — i~~ It must be noted that the reported values of measured volumetric strain, total (ε_{vol}) and maximum ($\varepsilon_{\text{vol,max}}$), correspond to the entire 3D volume. In all scans a more pronounced expansion is measured on the location of the lowest pre-existing micro-fissure ($\varepsilon_{\text{vol,max}}$). Only after 2 months of CO_2 exposure (scan 03) a slight expansive activity may be measured around

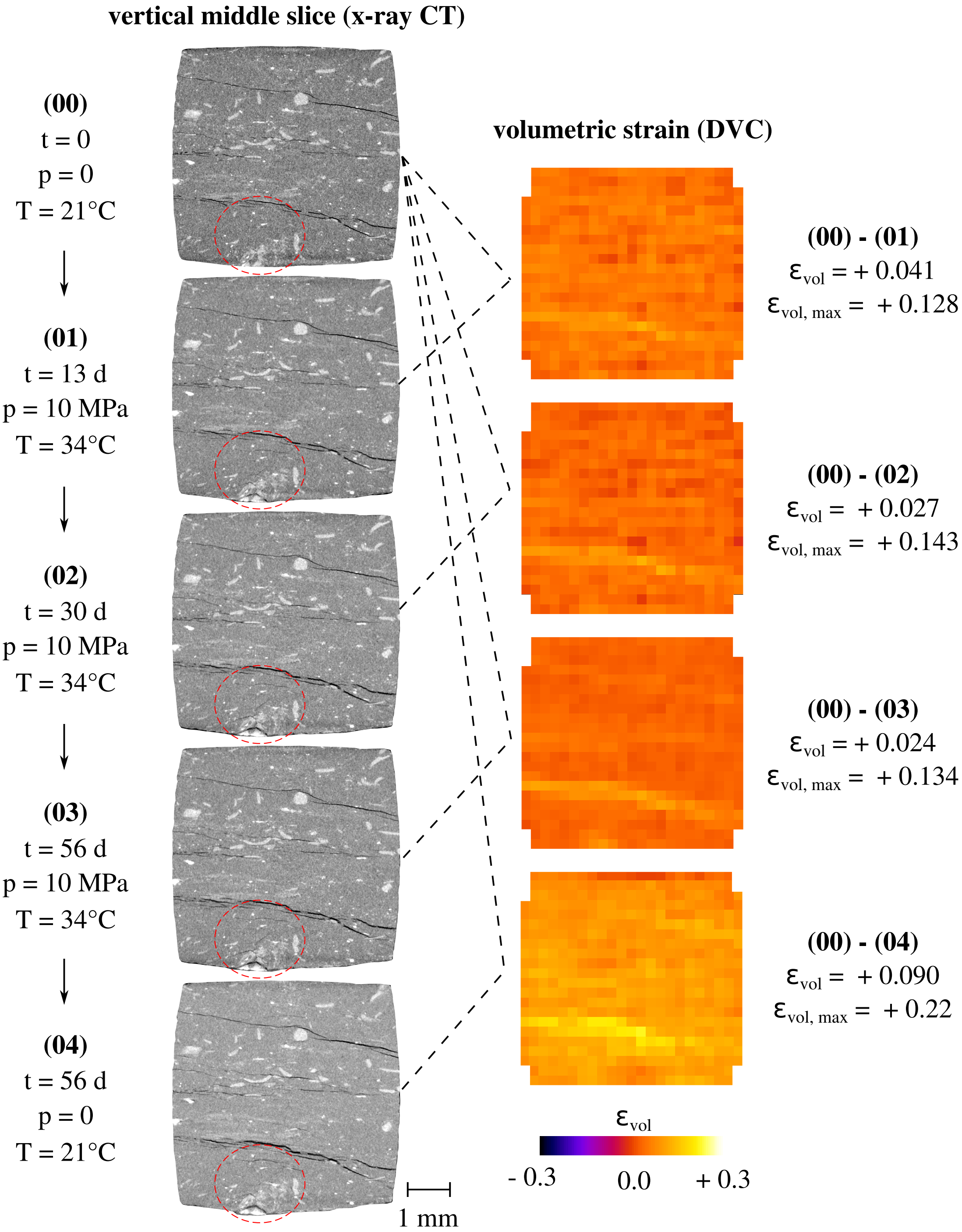

Figure 7: Volumetric response ~~of the middle vertical slice~~ of the Opalinus Clay sample in time after exposure to supercritical CO_2 – left: middlde vertical slice of the x-ray CT image with highlighted in red the zone of increased cracking activity, right: corresponding map of volumetric strain from DVC analysis

the othe two pre-existing ones. The overall expansive response of the sample (positive ε_{vol}) is clearly dominated by the expansion of the fissures. ~~that remains mostly constant in time. For the rest of the material it is hard to observe a clear pattern, nevertheless~~ A distinct pattern is absent in the rest of the material, but the calculated volumetric strain reveals an initial expansion ($\varepsilon_{\text{vol}_{00\text{-}01}} = +\,0.041$) that in time reduces ($\varepsilon_{\text{vol}_{00\text{-}02}}$ = + 0.027) and stabilises ($\varepsilon_{\text{vol}_{00\text{-}03}}$ = + 0.024). Finally, upon pressure decrease, the material expands in a more pronounced way ($\varepsilon_{\text{vol}_{00\text{-}03}}$ = + 0.090), not only at the lower crack zone but everywhere in the sample due to stress relaxation.~~, as explained in the following.~~ These results are discussed in detail in a following section.

~~The interpretation of this response is not straightforward since the sample is subjected to complex THMC boundary conditions. In theory, the application of constant pressure equilaterally and directly in contact with a fully water saturated sample is not supposed to affect the applied effective stress that should remain zero. In other words, since CO_2 is injected equilaterally in the unjacketed sample, the concept of effective stress is not valid, neither is the concept of hydraulic fracturing with the increase of pore pressure as it is the same with the applied skeleton pressure. However, the presence of pre-existent fissures suggests that the sample cannot be realistically fully saturated and that matric suction must be present locally in the fissured and partially saturated zones. Upon high pressure CO_2 exposure suction breakdown occurs locally (decrease of effective stress) and the sample swells until stabilisation at full saturation — water + CO_2. This interpretation can confirm the initial volumetric activity that eventual stabilises in time.~~

~~Local modification of the effective stress is not the only mechanism that may take place upon exposure of a shale sample to supercritical CO_2. Temperature increase (34°C) induces thermal expansion to the sample that can indeed justify the rather isotropic expansion measured in scan 01. Another important aspect that has been little discussed in the literature is the dessication of the material when in contact with CO_2. Indeed, the pore water of the material evaporates in the anhydrous CO_2 resulting desaturation which can result to further crack opening (expansion) and pore collapse in the clay matrix. This dessication effect could explain the lower volumetric expansion in time until eventual equilibrium. This little discussed interaction can occur in real field conditions at the bottom of the caprock formation in contact with the buoyant CO_2, leading to partial desaturation of the caprock and threaten its mechanical integrity and sealing capacity.~~

~~To better understand the impact of the afore mentioned coupled THM mechanisms, the evolution of the fissures volume in the different scans is presented in Fig. 8. For their calculation, the same GV threshold has been used for all the normalised scans. Once again, segmentation of shale images is a difficult exercise, the optimisation of which is out of the scope of this study. The obtained results are~~

~~considered sufficient to demonstrate the overall behaviour of the material. While the volumetric increase of the pre-existing fissures has already been identified from the calculated volumetric maps of the entire sample, Fig. 8 clearly demonstrates the creation and propagation of a new family of fissures at the bottom of the sample. These new fissures demonstrate in a very clear way the dessication effect of anhydrous CO_2 explained above. Additional chemo-mechanical mechanisms may contribute to the initiation of these micro-fissures that are impressively localised in a calcite-rich area at the bottom of the sample (see x-ray images in Fig. 8). Eventual dissolution aspects are hard to interpret since preferential fissuring patterns in calcite-rich zones may primarily be due to increased porosity between the calcite and the clay mineral interface (as shown in Fig. 6.~~

4.2 CO2 uptake

The visualisation and quantification of CO_2 penetration in the material is presented in this part, based on analysis of the GV evolution of the x-ray images after correction for volumetric strain (Stavropoulou et al., 2020). ~~After the in-depth analysis of the microstructural response of the caprock material during direct contact with supercritical CO_2, an attempt to visualise and quantify the CO_2 penetration in the material is attempted in this part of the study. The analysis is based on the evolution of the x-ray images GVs after correction due to volumetric strain as per Stavropoulou et al., (2020).~~ This approach is quite ~~ambitious~~ challenging in the context of CO_2 uptake, since the density variations due to supercritical CO_2 invasion are very slight (unlike the case of a denser fluid). This is why normalisation of the ~~images'~~ GVs is imperative for this kind of analysis (see Appendix).

~~Taking into account the measured strain field from the DVC analysis, the variation of the x-ray attenuation coefficient (μ_x) in time is corrected and measured. Volumetric strain results in density variation (and therefore μ_x variation) that is manifested in the GVs level of the deformed image via a linear relationship. A simple example to better understand this reasoning is the case of thermal expansion with no mass transfer, where the density of the material is expected to reduce, and consequently the attenuation field μ_x or GVs to decrease proportionally to the change in density. Any additional GV variation is therefore assumed to be due to additional mass transfer (gain or loss); in this work due to CO_2 uptake. According to Stavropoulou et al., (2020), the attenuation variation of a sample is calculated as a function of the mechanical volumetric strain assuming mass conservation:~~

$$\Delta\mu = -\varepsilon_v \cdot \mu_0 \tag{2}$$

~~where ε_v is the measured volumetric strain of the sample and μ_0 is the initial attenuation of the image (before loading).~~

~~In order to measure the additional changes of GVs due to mass transfer, the calculated strain field is applied on the reference image (scan 00), while taking into account the corresponding GV correction. Then, simple subtraction of the deformed image (with corrected GVs due to volumetric variation) from the corresponding original image (e.g. 01 minus 00-def-to-01) results in the uptake or loss of mass. The result of this analysis is presented in Fig. 8, where the chosen colourbar represents density (in terms of GV) increase (red) or decrease (blue).~~

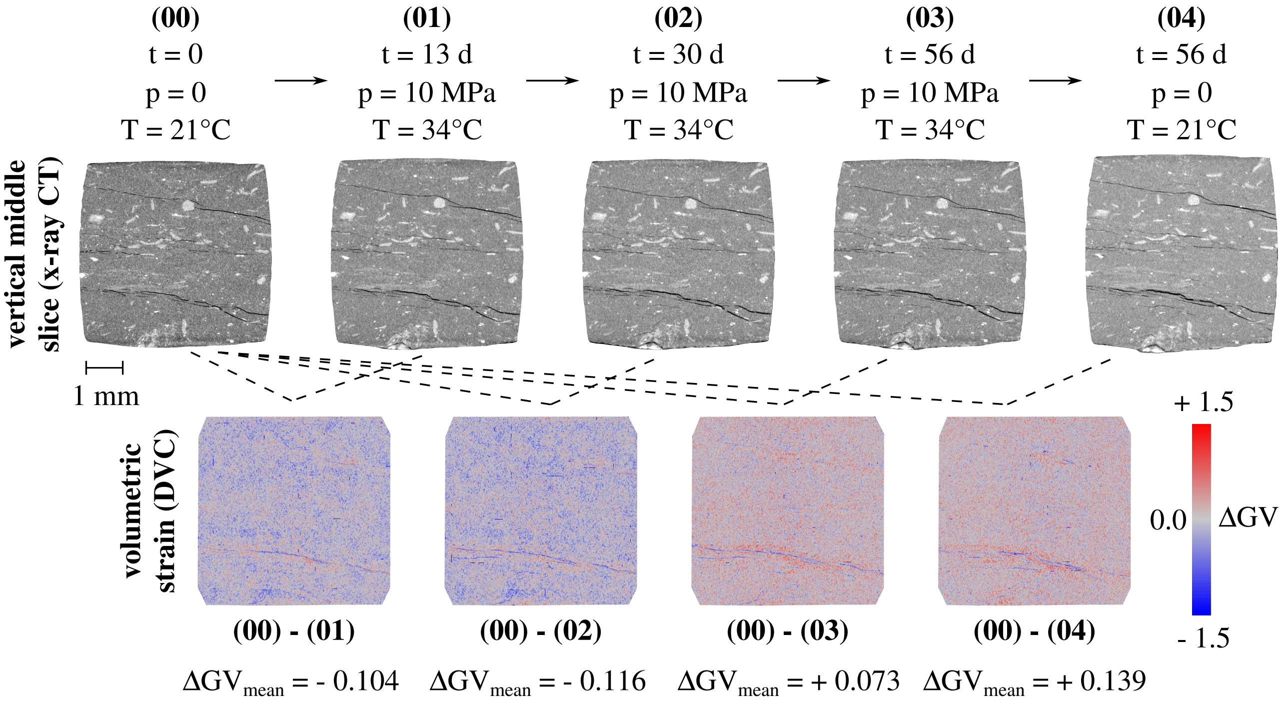

Figure 8: Fields of the grey value changes of the caprock material in time after removing the changes due to volumetric strain – the chosen colourbar represents density (in terms of GV) increase (red) or decrease (blue)

The maps of the GV variation are presented in Fig. 8. ~~show a density decrease overall during the first month of exposure (00-01 and 00-02).~~ A density decrease is observed overall during the first month of exposure (00-01 and 00-02). ~~This response can be supported by the desaturation discussed~~

~~earlier; in fact, invasion of anhydrous CO_2 in the material partially occurs through water evaporation, therefore the material is filled up with a fluid of lower density. While~~ Even though these results are somewhat noisy, ~~for precise conclusions, nevertheless~~ a more pronounced ~~*density decrease*~~ density decrease is obtained , ~~during the first month~~ at the lower part of the sample where ~~*crack initiation*~~ crack initiation occurs. On the other hand, around the zones of the ~~*pre-existing fissures*~~ pre-existing fissures a ~~*density increase*~~ density increase is measured~~; i~~ In this case the ~~non saturated~~ zones around the fissures ~~might have been~~ are possibly filled in with CO_2. It has to be noted that this approach is even less accurate around ~~in~~ the crack locations. This is because the obtained fields are the result of the subtraction between the initial least fissured image (00) with a future deformed image (e.g. 02) that has more fissures. ~~t~~ The application of the calculated deformation field on 00 cannot create these new fissures, ~~this is why directly on the fissures the density will be always decreasing (blue)~~ and therefore, the density will always be decreased in the direct vicinity of the fissures (blue).

Two months after CO_2 exposure, the overall density of the material ~~eventually increases in a relatively homogeneous way~~ increases homogeneously, if not ~~with~~ more noticeably around the lower pre-existing fissure. It is interesting to notice that between scans 02 and 03 the volumetric activity that was measured is almost negligible. This density increase under constant volume reveals the saturation of the material with CO_2. ~~Indeed, u~~Unlike the previous two fields, here the material seems to be in equilibrium indicating that CO_2 has invaded it in its entity. Final CO_2 pressure release (00-04) leaves the sample with an overall increased density, in particular at the zones around the fissures and at the bottom. This final result may indicate chemo-mechanical or CO_2 trapping phenomena that occurred during the two months exposure. The different results are discussed in the following section. ~~This is a first attempt to visualise CO_2 invasion in a caprock material and even though it is quantitative in terms of GV levels, their physical interpretation in terms of e.g. actual CO_2 volume increase or water decrease requires further studies and measurement for the calibration of the different phases' GVs~~.

5 Discussion

5.1 Long-term CO2 exposure

Long-duration exposure of Opalinus Clay to CO_2 showed micro-structural modifications, both in the clay matrix and the carbonate zones in the material. When CO_2 is placed in contact with the pore water of the shaly caprock material, it results in acidification of the pore fluid – by means of diffusion – and therefore in alteration of the chemical equilibrium. For instance, pre-existing carbonate crystals might be dissolved by the acidic fluid and enhance the transport properties of the material (Busch et al., 2008; Espinoza et al., 2011; Jia et al., 2018).

In this study, the identified cracks in the calcite zones of Opalinus Clay after long-term interaction with CO_2 are associated to dissolution effects. Even though calcite dissolution has not been previously observed to result in fissuring, the fissures in the calcite zones of the material reveal a localised activity within these zones. Calcite dissolution in shales is mainly identified indirectly by post-mortem analysis either of injected fluids or solid samples. In this work, the visualisation of large calcite inclusions allow the observation of micro-structural modifications that occur locally, within the area of interest (i.e. the calcite zones). Possible desaturation of the sample is not likely to explain the creation of these localised fissures, since dessication cracks in shales appear mainly within the clay matrix or at the interface of the clay matrix with other inclusions (calcite, pyrite etc.). Fissuring in the clay matrix is however not observed even after total pressure release (unconfined conditions). On the contrary, the number of pre-existing fissures initially in the sample is reduced. This is additionally ensuring for the potential impact of progressive pressure loss during these 9 months of exposure. Pressure loss may result in desaturation and fissuring of the sample (usually parallel to the bedding orientation) that have not been observed at the given resolution of this study.

Fissure closure can be explained by means of hydromechanical self-sealing behaviour of the material under long-term confinement. The self-sealing response of shales is one of the main properties for which this material is studied as a potential sealing material in a broader context of underground storage, such as radioactive waste, CO_2 or hydrogen storage (Bossart et al., 2019; Di Donna et al., 2022, Yu et al., 2022). Hou et al., (2022) discussed the self-sealing response of caprock materials in terms of mineral precipitation. They showed that in illite-rich shale precipitation took place in quartz, i.e. Si-rich zones. In the current study, Si-rich zones are unfortunately not distinguishable from the either SEM or x-ray images. Prakash et al., (2022) pointed out a more pronounced precipitation activity in zones parallel to the direction of the bedding plane. This is in line with the identified orientation of fissures in the sample before and after confinement and CO_2 exposure. The pre-existing fissures that were parallel to the bedding orientation disappear, and the fewer fissures after long-term confinement and CO_2 exposure are in their majority no longer parallel to the bedding. Other works have shown that incorporation of supercritical CO_2 in micro-structural interlayers can induce the beneficial swelling of smectitic clays (Alemu et al., 2011; Busch et al., 2016). This aspect is discussed in more detail in the following section, in association to the measured volumetric response of the material.

Finally, it is not clear whether these new fissures are the result of further chemical reactions due to alteration of the pore fluid's pH, or whether they are related to mechanical impact from previous CO_2 breakthrough (see 3D volumetric response after breakthrough in Stavropoulou and Laloui, 2022). In either case, this result points out a potential rearrangement of the fissure network after long-term CO_2 exposure that has not been previously discussed. Most importantly, these results on the micro-structural modifications show how little we still know regarding the coupled long-term THMC response of the caprock/CO_2 interaction at the micro-scale and their implications to the large scale response. Longer-duration testing under realistic boundary conditions are required for a better understanding of the complex mechanisms that occur.

5.2 THMC response

The volumetric response of Opalinus Clay to direct equilateral exposure of supercritical CO_2 presented an increased activity around the zones of the three pre-existing micro-fissures. First, an overall volumetric expansion was measured (scan 01) resulting from the temperature increase for the application of supercritical conditions, i.e. from ambient 25°C to 34°C. This initial expansion may be additionally related to smectite swelling upon exposure to supercritical CO_2 (Busch et al., 2016). Expansion was then followed by compaction until stabilisation of the volumetric strain in time, with some elevated values around the bottom fissure and the bottom of the sample.

The interpretation of this response is not straightforward since the sample is subjected to complex THMC boundary conditions. In theory, the application of constant pressure equilaterally and directly in contact with a water saturated sample is not supposed to affect the applied effective stress that should remain zero. In other words, since CO_2 is provided equilaterally on the unjacketed sample, the concept of effective stress is not valid, neither is the concept of hydraulic fracturing with the increase of pore pressure, as it is the same with the applied skeleton pressure. However, the presence of pre-existing fissures suggests that the sample is in reality not fully saturated and that matric suction (negative pore pressure) must be present locally in the fissured and partially saturated zones. Upon introduction of high pressure CO_2, suction breakdown occurs locally (decrease of effective stress) and the sample swells until stabilisation at full saturation – water + CO_2. This hydromechanical interpretation can confirm the initial volumetric activity that eventually stabilises in time. Zhang et al. (2018) have previously addressed evolution of the axial effective stress of partially water saturated montmorillonite upon injection of supercritical CO_2 (10 MPa and 44°). They evaluated the swelling stresses of the material under different levels of confinement and attributed them to expansive smectite response. Otherwise, smectite swelling has been mostly observed under unconfined conditions (Schaef et al., 2012; De Jong et al., 2014; Michels et al. 2015). In this study, the boundary conditions are different but closer to unconfined conditions, with zero effective stress globally but not necessarily locally.

Another important aspect that has been discussed little in the literature is the dessication of the material when in contact with CO_2 (Espinoza and Santamarina, 2010; Miri and Hellevang, 2016; Cui et al. 2021). The pore water of the material evaporates in the anhydrous CO_2 resulting desaturation which can result to further crack opening (expansion) and pore collapse in the clay matrix. Dessication could explain the lower volumetric expansion in time until eventual equilibrium. This little discussed interaction can occur in real field conditions at the bottom of the caprock formation in contact with the buoyant CO_2, leading to partial desaturation of the caprock and threaten its mechanical integrity and sealing capacity.

To better understand the impact of the afore mentioned coupled THM mechanisms, the volumetric evolution of the fissures in the different scans is calculated and presented in Fig. 9. For this calculation, the same GV threshold has been used for all the normalised scans. Whereas the volumetric increase of the pre-existing fissures has already been identified from the calculated volumetric maps of the entire sample, Fig. 9 reveals the creation and propagation of a new family of fissures at the bottom of

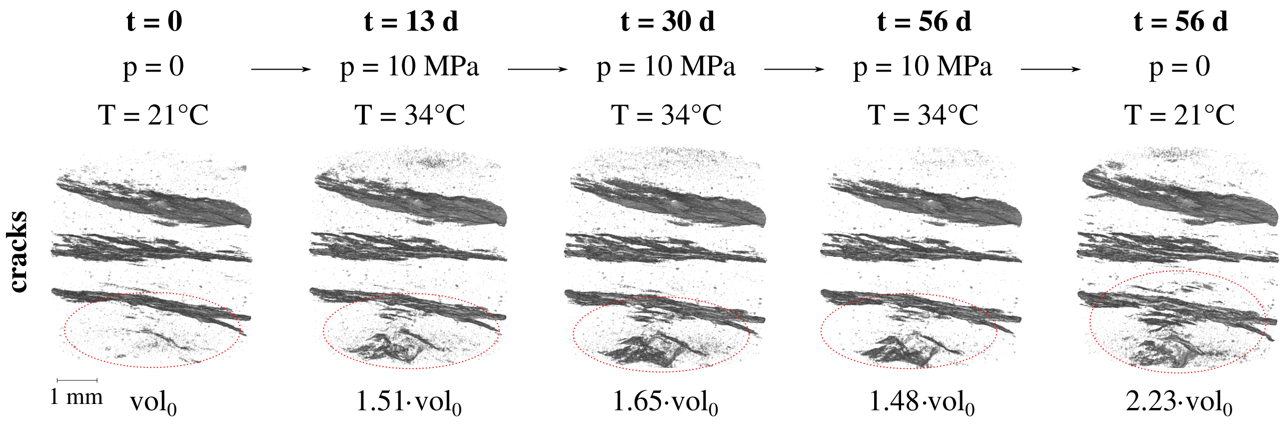

Figure 9: Evolution of pre-existing fissures and appearance of new ones (encircled zones) after direct exposure to supercritical CO_2 (illustration in 3D)

the sample. These new fissures demonstrate in a clear way the dessication effect of anhydrous CO_2 explained above. Additional chemo-mechanical mechanisms (such as dissolution) may contribute to the initiation of these micro-fissures that are noticeably localised in a calcite-rich area at the bottom of the sample (see x-ray images in Fig. 7). Eventual dissolution aspects are hard to interpret since preferential fissuring patterns in calcite-rich zones may be due to the increased porosity between the calcite interfaces and the clay mineral interface (as shown in Fig. 6).

Phenomena related to pore fluid alteration, e.g. water evaporation in the anhydrous CO_2, alteration of the pore fluid pH due to CO_2 diffusion or eventual invasion of CO_2 in the material, have been addressed by measuring the evolution of the density (GV) of the material in time while accounting for the corresponding volumetric strain. The density decrease that is observed overall during the first month of exposure (see Fig. 8 00-01 and 00-02) can be explained by the desaturation of the sample discussed earlier. Invasion of anhydrous CO_2 in the material partially occurs through water evaporation, therefore the material is filled up with a fluid of lower density. The following density increase, can be attributed to both pore fluid changes and CO_2 uptake in the material. Geochemicanl interactions between the invading supercritical CO_2 and the solid matrix of the material cannot be easily argued from the obtained results. For example, potential swelling of smectite has already been accounted and corrected in the given density maps and all density changes are related to mass-related changes (uptake or loss). This is a first attempt to visualise CO_2 invasion in a caprock material and even though it is quantitative in terms of GV levels, the physical interpretation in terms of e.g. actual CO_2 volume increase or water decrease requires further studies and measurement for the calibration of GVs of the different phases.

5.3 Implications for geological CO2 storage

In this work, a series of coupled phenomena that take place in a shaly caprock material have been addressed and discussed based on qualitative and quantitative measurements of 3D x-ray tomography images. The various THMC mechanisms that have been demonstrated, are related to some extent to the equivalent testing conditions: stress state, CO_2 pressure and time exposure, water saturation/dessication, mineral dissolution and precipitation. However, field conditions are different than these testing conditions. For instance, the levels of effective stress in a CO_2 storage site are much higher, in the order of 10 to 20 MPa (depending on the storage depth). Consequently, the stress state of the material has an impact on the appearance of fissures. The fissures in the calcite-rich zones of the material have been visualised in an unconfined sample state (scan taken after pressure release). Similarly, dessication fissures due to water evaporation in the invading anhydrous CO_2 might not manifest (at the given resolution) under elevated levels of effective stress. However, drying of the caprock due to interaction with undissolved CO_2, is a phenomenon that might take place at the interface between the reservoir and the caprock due to the buoyant tendency of CO_2. Dessication of the caprock can have implications that can threaten the caprock integrity and sealing capacity, for example, facilitate CO_2 breakthrough. The exact CO_2 breakthrough pathway in the caprock is not easy to predict because of the high micro-structural heterogeneity of the material. The connected pore space (including fissures) is supposed to drive flow and breakthrough phenomena, however, the different competing mechanisms (e.g. dessication, local effective stress modification) may result in the collapse of initially conductive pathways and the creation of new ones. There has been previous evidence of such phenomena in gas migration tests (Harrington et al. 2012; Cuss et al., 2014). The results of this study and their interpretation, demonstrate the importance of considering the different localised effects for a better understanding of the long-term response of shales in the context of geological CO_2 storage. Macroscopic or averaged measurements and observations that do not take into account the micro-structural heterogeneity of shales, are limited for the development representative constitutive and numerical models.

6 Conclusions

In this work the interaction between the Opalinus Clay, a caprock representative material, with CO_2 is studied with x-ray tomography imaging. The different results and observations reveal the complex response of this material due to multiple coupled phenomena that occur in parallel. Exposure to supercritical CO_2 implies temperature increase of the material that results in thermal expansion (TM coupling). This expansion leads to inevitable desaturation of the material (TH coupling). At the same time, the live observation of the caprock material in time revealed another important aspect when anhydrous CO_2 is in contact with the water saturated sample.~~; t~~ The pore water evaporates in the anhydrous CO_2 causing further dessication of the material that starts fissuring. Fissures, whether pre-existing in the material or new ones, play an important role on the CO_2/caprock interaction. They drive most of the volumetric and hydraulic phenomena~~;~~: swelling, desaturation, uptake, breakthrough. In the field, fissures in the caprock formation could found around the injection wellbore or fault zones, but ~~T~~ their impact is still not well understood.~~, in particular under realistic field conditions.~~

The long-term impact of CO_2 on the micro-structure of ~~the~~ a shaly material (the Opalinus Clay) is for the first time visualised with x-ray tomography on a solid sample and under non-extreme temperature and pressure conditions (< 40°C and 10 MPa respectiveley). Fissuring of calcite-rich zones after 9 months of CO_2 exposure is associated to dissolution-related effects (CM coupling). ~~Calcite dissolution is identified in carbonate-rich zones that after 9 months of exposure they were fissured (CM coupling)~~. The mineralogical composition of these denser inclusions in the x-ray images has been confirmed from SEM-EDX measurements. Segmentation and labelling of the inclusions before and after long-duration CO_2 exposure confirmed an increased number of inclusions due to ~~breakage (dissolution)~~ fissuring, the mean orientation of which did not significantly evolve. A similar analysis has been made on the fissure network in the clay matrix of the sample before and after long-term exposure. The principal crack orientation in the sample is initially parallel to the bedding orientation of the shaly material. These fissures close with the application of confinement as shown in ~~(~~Stavropoulou and Laloui, (2022) but ~~very interestingly they~~ do not re-appear 9 months later, after pressure release. This result demonstrates the self-sealing response of Opalinus Clay that can be attributed to a series of mechanisms: long-term hydromechanical loading (HM coupling), expansive smectitic response, mineral precipitation of Si-rich zones (CM couplings). In addition to the closure of pre-existing fissures, the ~~9 months~~ x-ray scan after 9 months revealed the appearance of ~~some~~ new micro-fissures in the clay matrix (other than the fissures in the calcite zones), surprisingly in a perpendicular direction to the bedding. This aspect of potential re-arrangement of the fissure network of the material is demonstrated for the first time and could be ~~due~~ related to additional chemo-mechanical mechanisms within the clay matrix or related to CO_2 breakthrough that due to self-sealing of the initial micro-fissures initiated a new optimal pathway throughout the sample. The preferential pathway of CO_2 breakthrough is not yet well understood in such heterogeneous microstructures and may induce fissuring of different orientation than the in-situ bedding.

Finally, the CO_2 uptake in the caprock material has been investigated by combining the calculated strain fields and the GV variation of the acquired x-ray images. CO_2 penetration in the sample has been identified two months after initial exposure. It is hard to interpret the multi-phase fluid interaction in the porous space of the material prior to two months due to the multiple THMC phenomena that take place simultaneously and often counteract each other. It is ~~interesting to note~~ significant that after CO_2 release the density of the sample remained increased compared to the initial two months earlier, revealing potential CO_2 trapping in the material.

Figure 10 ~~sums up~~ highlights the different coupled mechanisms that have been identified in this work to occur during the CO_2/caprock interaction. These topics require undoubtedly further investigation with long-term experiments under continuously monitored conditions. Analysis of the response using a non-destructive tool, i.e. x-ray tomography allows the 3D study of the material locally, in zones where the different phenomena are prone to occur ~~while under realistic conditions~~. For instance, the evolution of calcite inclusions within the sample or sealing of pre-existing fissures in the clay matrix are visualised and quantified locally in the sample, unlike previous studies where such interactions have been discussed from more macroscopic/averaged results. The study of small shale samples has significantly contributed to the better understanding of the various coupled phenomena,~~;~~ first by achieving better time resolutions, ~~under non-extreme temperature and pressure conditions~~, and then by studying the ~~material's~~ response of the material under high spatial resolutions in 3D ~~that revealed~~, revealing mechanisms previously undetectable with conventional testing methods and resolutions. These phenomena include the volumetric reponse and water evaporation during exposure to supercritical CO_2, the localised chemo-mechanical interactions in calcite-rich zones, the CO_2 uptake

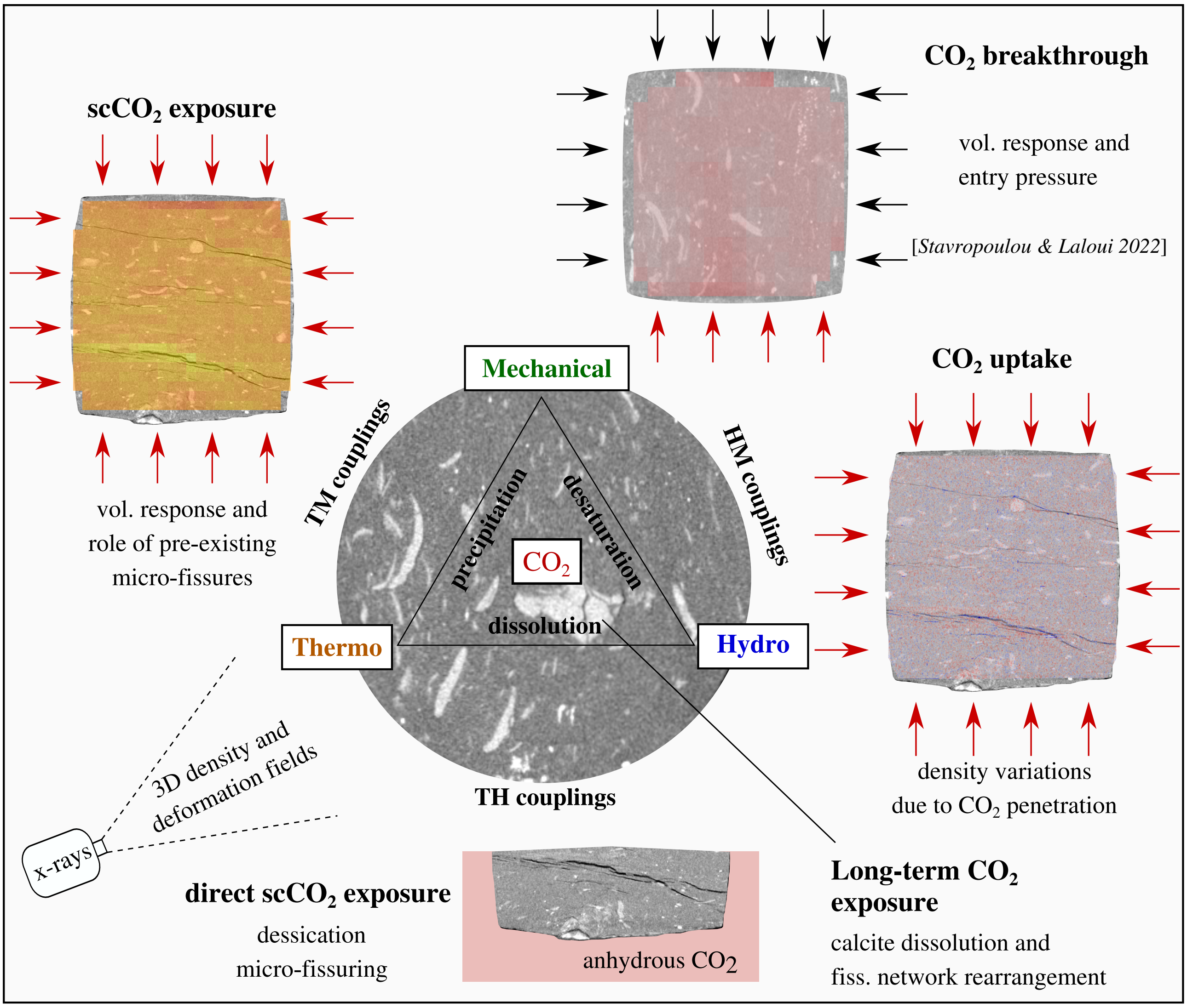

Figure 10: Coupled THMC mechanisms studied with in situ x-ray imaging on small size shale samples

and the role of micro-fissures in the material, and the volumetric response upon CO$_2$ breakthrough.

7 Data availability

The 3D x-ray images that have been used in this paper are provided online in Zenodo [link TBC]. Additional data or results can be provided by the Authors upon reasonable request.

8 Acknowledgements

This study has taken place in the frame of the Spark SNSF CRSK-2_196559 project. The Authors wish to thank the PIXE platform (EPFL) for the assistance during the x-ray tomography scans, as well as the Mont Terri laboratory and SwissTopo for providing the tested Opalinus Clay material.

Appendix A: Normalisation of x-ray tomographies

For the analysis of the attenuation evolution of the images, the different scans are normalised using always as reference scan 00. The objective of this normalisation is to set to zero the voxels that correspond to void in order to be able to more reliably detect density variations. The normalisation is performed considering the parts of the image that are not supposed to vary in density with time~~;~~ i.e. PEEk and Aluminium. Since the void attenuation is changing with the introduction of CO_2, the ratio of the greyvalues (GV) between Aluminium, PEEK and air is considered constant as shown in Fig. A1.

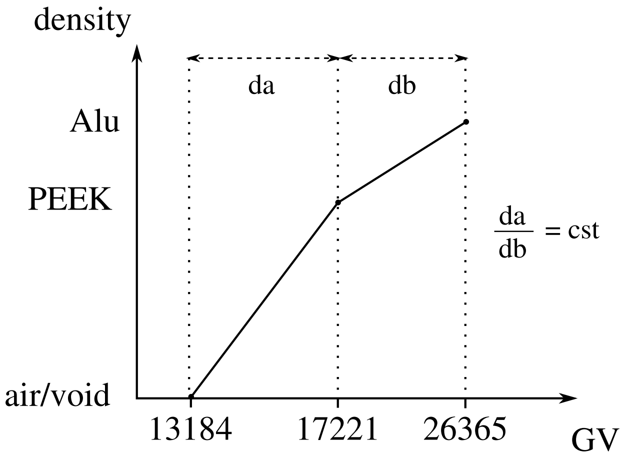

Figure A1: Measured greyvalues as a function of corresponding density in scan 00

GV (32b)	Void	PEEK	Aluminium	da	db	da/db
00	13184 (832)	17221 (833)	26365 (900)	4037	9144	0.44149
01	**13113**	17195 (841)	26442 (910)	**4082**	9247	0.44149
02	**13191**	17237 (839)	26403 (907)	**4046**	9166	0.44149
03	**13450**	17330 (613)	26119 (693)	**3880**	8789	0.44149
04	**13445**	17287 (602)	25990 (699)	**3842**	8703	0.44149

Table A1: Measured (normal font) and calculated (bold font) mean greyvalues (and standard deviation/error in the parenthesis) of the parts of the scan that are not expected to vary in density with time for the normalisation of the images

This ratio is calculated from the reference scan 00 (first row of Table A1) and considered constant in order to deduce the air greyvalue of the rest of the scans. The computed GV of air (first column of Table A1) is then subtracted from each scan, which is then divided by the corresponding PEEK value so that PEEK average value is 1 for the sake of simplicity. The histogram of scan 00 after normalisation is shown in Fig. A2-a, while the histogram after CO_2 introduction (scan 003) is changed to that in Fig. A2-b. The GV normalisation of the different scans can improve the volumetric analysis (DVC) and it is indispensa1ble for the detection of density variations.

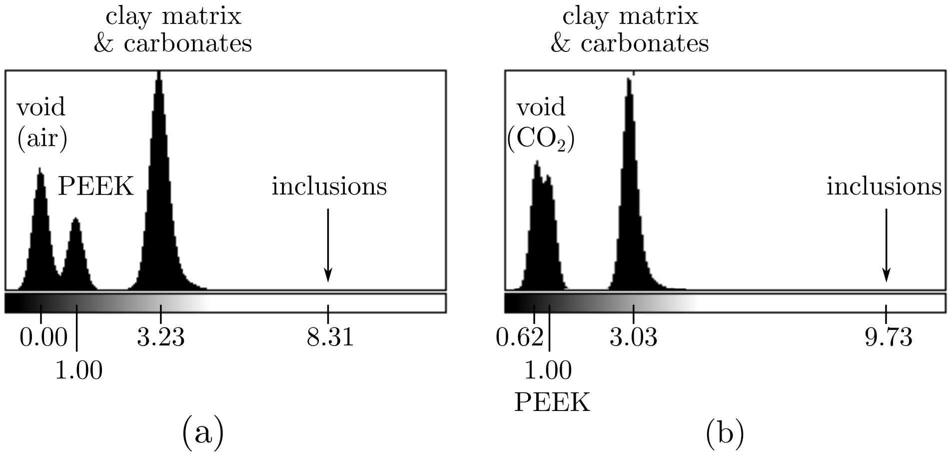

A2: Greyvalues histogram of normalised (a) scan 00 (no CO_2) and (b) scan 01 (with CO_2)

Appendix B: Segmentation of the x-ray images

The different steps for the segmentation for the different types of phases are illustrated in Fig. B1. First, a bilateral filter is applied on the original image in order to smoothen the zones of similar phases and sharpen the edges between different phases (Fig. B1-a).

The distributions of the GV levels before and after the application of this filter are plotted in Fig. B2.~~; a more narrow~~ A narrower distribution is obtained after the bilateral filter, providing more precision for the selection of each GV range for the segmentation of the different phases. The resulted segmented slices of the inclusions and the micro-fissures after the application of a threshold GV range are shown in Fig. B1-b and c, respectively. In the case of the inclusions, a double cycle of dilation and erosion of the binary image has been applied in order to reduce noise. This is not possible for a further noise reduction of the ~~noise~~ of the fissures segmented image due to their 1 pixel thickness.

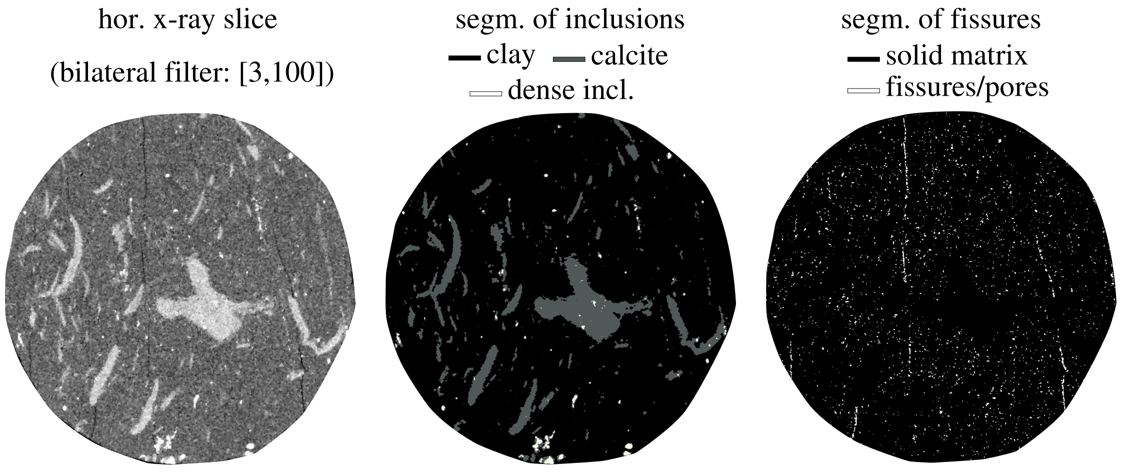

(a) (b) (c)

Figure B1: Horizontal slices after the (a) application of a bilateral filter, (b) segmentation of the two types of inclusions (calcite and denser inclusions), (c) micro-fissures

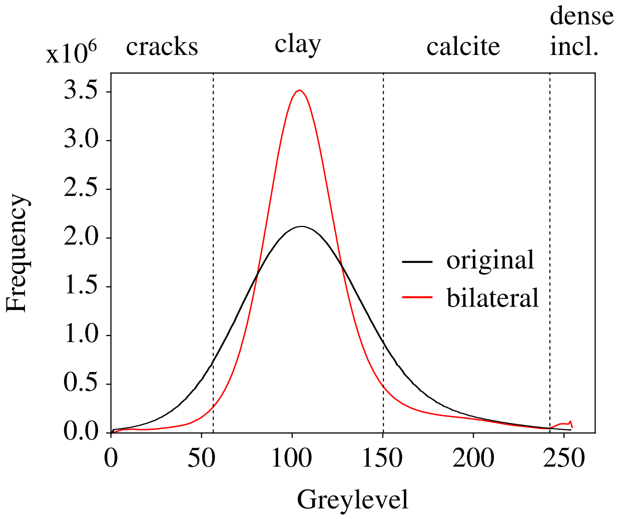

B2: Greyvalues histogram of the original horizontal x-ray slice and after the application of bilateral filter of Fig. B2 (a)

References

[1] Alemu, B. L., Aagaard, P., Munz, I. A., & Skurtveit, E.: Caprock interaction with CO2: A laboratory study of reactivity of shale with supercritical CO2 and brine. Applied Geochemistry, 26(12), 1975-1989, `https://doi.org/10.1016/j.apgeochem.2011.06.028`, 2011.

[2] Amann-Hildenbrand, A., Bertier, P., Busch, A., & Krooss, B. M.: Experimental investigation of the sealing capacity of generic clay-rich caprocks. International Journal of Greenhouse Gas Control, 19, 620-641,`https://doi.org/10.1016/j.ijggc.2013.01.040`, 2013

[3] Armitage, P. J., Worden, R. H., Faulkner, D. R., Aplin, A. C., Butcher, A. R., & Iliffe, J.: Diagenetic and sedimentary controls on porosity in Lower Carboniferous fine-grained lithologies, Krechba field, Algeria: A petrological study of a caprock to a carbon capture site. Marine and Petroleum Geology, 27(7), 1395-1410, `https://doi.org/10.1016/j.marpetgeo.2010.03.018`, 2010.

[4] Armitage, P.J., Faulkner, D.R., & Worden, R.H.: Caprock corrosion. Nat. Geosci., 6, 79–80, 2013.

[5] Bedford, J., Fusseis, F., Leclère, H. Wheeler, J., & Faulkner, D.: A 4D view on the evolution of metamorphic dehydration reactions. Scientific Reports, 7(1), 1-7. `https://doi.org/10.1038/s41598-017-07160-5`, 2017.

[6] Birmpilis, G., Hall, S. A., Lages, S., & Dijkstra, J.: Monitoring of the nano-structure response of natural clay under mechanical perturbation using small angle X-ray scattering and digital image correlation. Acta Geotechnica, 14(6), 1965-1975, `https://doi.org/10.1007/s11440-019-00832-8`, 2019.

[7] Birmpilis, G., & Dijkstra, J.: Testing sensitive clays through time and length scales. IOP Conference Series: Earth and Environmental Science, 710, 012021, `https://doi.org/10.1088/1755-1315/710/1/012021`, 2021.

[8] Birmpilis, G., Andò, E., Stamati, O., Hall, S. A., Gerolymatou, E., & Dijkstra, J.: Experimental quantification of 3D deformations in sensitive clay during stress-probing, Géotechnique, 1-12, `https://doi.org/10.1680/jgeot.21.00114`, 2022.

[9] Bossart, P. & Thury, M.: Characteristics of the Opalinus clay at Mont Terri, Reports of the Swiss Geological Survey 3, 2011.

[10] Busch, A., Alles, S., Gensterblum, Y., Prinz, D., Dewhurst, D. N., Raven, M. D., Stanjek, H., & Krooss, B. M.: Carbon dioxide storage potential of shales, International journal of greenhouse gas control, 2(3), 297-308, `https://doi.org/10.1016/j.ijggc.2008.03.003`, 2008.

[11] Busch, A., Bertier, P., Gensterblum, Y., Rother, G., Spiers, C. J., Zhang, M., & Wentinck, H. M.: On sorption and swelling of CO2 in clays. Geomechanics and Geophysics for Geo-energy and Geo-resources, 2(2), 111-130, `https://doi.org/10.1007/s40948-016-0024-4`, 2016.

[12] Crisci, E., Ferrari, A., Giger, S. B., & Laloui, L.: Hydro-mechanical behaviour of shallow Opalinus Clay shale, Engineering Geology, 251, 214-227, `https://doi.org/10.1016/j.enggeo.2019.01.016`, 2019.

[13] Cui, G., Zhu, L., Zhou, Q., Ren, S., & Wang, J.: Geochemical reactions and their effect on CO2 storage efficiency during the whole process of CO2 EOR and subsequent storage. International Journal of Greenhouse Gas Control, 108, 103335, `https://doi.org/10.1016/j.ijggc.2021.103335`, 2021.

[14] Cuss, R., Harrington, J., Giot, R., & Auvray, C. : Experimental observations of mechanical dilation at the onset of gas flow in Callovo-Oxfordian claystone. Geological Society, London, Special Publications, 400(1), 507-519, `https://doi.org/10.1144/SP400.26`, 2014.

[15] Delage, P., & Tessier, D.: Macroscopic effects of nano and microscopic phenomena in clayey soils and clay rocks, Geomechanics for Energy and the Environment, 27, 100177, `https://doi.org/10.1016/j.gete.2019.100177`, 2021.

[16] Delage, P., & Belmokhtar, M.: Drained triaxial testing of shales: insight from the Opalinus Clay, Acta Geotechnica, 17(7), 2855-2874, 2022.

[17] De Jong, S. M., Spiers, C. J., & Busch, A.: Development of swelling strain in smectite clays through exposure to carbon dioxide. International Journal of Greenhouse Gas Control, 24, 149-161, `https://doi.org/10.1016/j.ijggc.2014.03.010`, 2014.

[18] Desbois, G., Höhne, N., Urai, J. L., Bésuelle, P., & Viggiani, G.: Deformation in cemented mudrock (Callovo-Oxfordian Clay) by microcracking, granular flow and phyllosilicate plasticity: insights from triaxial deformation, broad ion beam polishing and scanning electron microscopy, Solid Earth, 8(2), 291, `https://doi.org/10.5194/se-8-291-2017`, 2017.

[19] Di Donna, A., Charrier, P., Dijkstra, J., Andò, E., & Bésuelle, P. (2022). The contribution of swelling to self-sealing of claystone studied through x-ray tomography. Physics and Chemistry of the Earth, Parts A/B/C, 127, 103191.

[20] Elkady, Y., & Kovscek, A. R.: Multiscale study of CO2 impact on fluid transport and carbonate dissolution in Utica and Eagle Ford shale, Journal of Petroleum Science and Engineering, 195, 107867, `https://doi.org/10.1016/j.petrol.2020.107867`, 2020.

[21] Espinoza, D. N., Kim, S. H., & Santamarina, J. C.: CO2 geological storage - Geotechnical implications, KSCE Journal of Civil Engineering, 15(4), 707-719, `https://doi.org/10.1007/s12205-011-0011-9`, 2011.

[22] Espinoza, D. N., & Santamarina, J. C.: Water-CO2-mineral systems: Interfacial tension, contact angle, and diffusion – Implications to CO2 geological storage. Water resources research, 46(7), `https://doi.org/10.1029/2009WR008634`, 2010.

[23] Favero, V., Ferrari, A., & Laloui, L.: On the hydro-mechanical behaviour of remoulded and natural Opalinus Clay shale, Engineering Geology, 208, 128-135, `https://doi.org/10.1016/j.enggeo.2016.04.030`, 2016.

[24] Favero, V., Ferrari, A., & Laloui, L.: Thermo-mechanical volume change behaviour of Opalinus Clay, International Journal of Rock Mechanics and Mining Sciences, 90, 15-25, `https://doi.org/10.1016/j.ijrmms.2016.09.013`, 2016.

[25] Favero, V., & Laloui, L.: Impact of CO2 injection on the hydro-mechanical behaviour of a clay-rich caprock, International Journal of Greenhouse Gas Control, 71, 133-141, `https://doi.org/10.1016/j.ijggc.2018.02.017`, 2018.

[26] Hadian, P., & Rezaee, R.: The Effect of Supercritical CO2 on Shaly Caprocks, Energies, 13(1), 149, `https://doi.org/10.3390/en13010149`, 2020.

[27] Harrington, J. F., Milodowski, A. E., Graham, C. C., Rushton, J. C., & Cuss, R. J.: Evidence for gas-induced pathways in clay using a nanoparticle injection technique. Mineralogical Magazine, 76(8), 3327-3336, `Harrington`, 2012.

[28] Hashemi, S. S., & Zoback, M. D.: Permeability evolution of fractures in shale in the presence of supercritical CO2, Journal of Geophysical Research: Solid Earth, 126(8), e2021JB022266, `https://doi.org/10.1029/2021JB022266`, 2021.

[29] Hou, L., Yu, Z., Luo, X., & Wu, S.: Self-sealing of caprocks during CO2 geological sequestration. Energy, 252, 124064, `https://doi.org/10.1016/j.energy.2022.124064`, 2022.

[30] Houben, M. E., Desbois, G., & Urai, J. L.: Pore morphology and distribution in the Shaly facies of Opalinus Clay (Mont Terri, Switzerland): Insights from representative 2D BIB–SEM investigations on mm to nm scale, Applied clay science, 71, 82-97., `https://doi.org/10.1016/j.clay.2012.11.006`, 2013.

[31] IPCC: Climate Change 2022: Mitigation of Climate Change, Contribution of Working Group III to the Sixth Assessment Report of the Intergovernmental Panel on Climate Change, Cambridge University Press, Cambridge, UK and New York, NY, USA. `https://doi.org/10.1017/9781009157926`, 2022.

[32] Jia, Y., Lu, Y., Elsworth, D., Fang, Y., & Tang, J.: Surface characteristics and permeability enhancement of shale fractures due to water and supercritical carbon dioxide fracturing, Journal of Petroleum Science and Engineering, 165, 284-297, `https://doi.org/10.1016/j.petrol.2018.02.018`, 2018.

[33] Kivi, I. R., Makhnenko, R. Y., & Vilarrasa, V.: Two-Phase Flow Mechanisms Controlling CO2 Intrusion into Shaly Caprock, Transport in Porous Media, 141(3), 771-798, `https://doi.org/10.1007/s11242-022-01748-w`, 2022.

[34] Li, C., & Laloui, L.: Impact of material properties on caprock stability in CO2 geological storage, Geomechanics for Energy and the Environment, 11, 28-41, `https://doi.org/10.1016/j.gete.2017.06.003`, 2017.

[35] Makhnenko, R. Y., Vilarrasa, V., Mylnikov, D., & Laloui, L.: Hydromechanical aspects of CO2 breakthrough into clay-rich caprock, Energy Procedia, 114, 3219-3228,`https://doi.org/10.1016/j.egypro.2017.03.1453`, 2017.

[36] Marschall, P., Horseman, S., & Gimmi, T.: Characterisation of gas transport properties of the Opalinus Clay, a potential host rock formation for radioactive waste disposal, Oil & gas science and technology, 60(1), 121-139, `https://doi.org/10.2516/ogst:2005008`, 2005.

[37] Menaceur, H., Delage, P., Tang, A. M., & Conil, N.: On the thermo-hydro-mechanical behaviour of a sheared Callovo-Oxfordian claystone sample with respect to the EDZ behaviour, Rock Mechanics and Rock Engineering, 49(5), 1875-1888, `https://doi.org/10.1007/s00603-015-0897-5`, 2016.

[38] Michels, L., Fossum, J. O., Rozynek, Z., Hemmen, H., Rustenberg, K., Sobas, P. A., Kalantzopoulos, G. N., Knudsen, K. D., Janek, M., Plivelic, T.S., & da Silva, G. J.: Intercalation and retention of carbon dioxide in a smectite clay promoted by interlayer cations. Scientific reports, 5(1), 1-9, `https://doi.org/10.1038/srep08775`, 2015.

[39] Minardi, A., Stavropoulou, E., Kim, T., Ferrari, A., & Laloui, L.: Experimental assessment of the hydro-mechanical behaviour of a shale caprock during CO2 injection, International Journal of Greenhouse Gas Control, 106, 103225, `https://doi.org/10.1016/j.ijggc.2020.103225`, 2021.

[40] Miri, R., & Hellevang, H.: Salt precipitation during CO2 storage – A review. International Journal of Greenhouse Gas Control, 51, 136-147, `https://doi.org/10.1016/j.ijggc.2016.05.015`, 2016.

[41] Mohajerani, M., Delage, P., Sulem, J., Monfared, M., Tang, A. M., & Gatmiri, B.: The thermal volume changes of the Callovo–Oxfordian claystone, Rock mechanics and rock engineering, 47(1), 131-142, `https://doi.org/10.1007/s00603-013-0369-8`, 2014.

[42] Prakash, R., Nguene, P.C.K., Noshadravan, A., & Abedi, S.: Chemical reactions of carbonate-rich mudstones with aqueous CO2 and their impacts on rock's local microstructural and chemo-mechanical properties, Journal of Natural Gas Science and Engineering, 103, 104587, `https://doi.org/10.1016/j.jngse.2022.104587`, 2022.

[43] Romero, E.: Controlled-suction techniques. 4o Simpósio Brasileiro de Solos Nâo Saturados. Gehling & F. Schnaid (eds.), Porto Alegre, Brasil, 535-542, 2021.

[44] Rutqvist, J.: The geomechanics of CO2 storage in deep sedimentary formations. Geotechnical and Geological Engineering, 30(3), 525-551, `https://doi.org/10.1007/s10706-011-9491-0`, 2012.

[45] Schaef, H. T., Ilton, E. S., Qafoku, O., Martin, P. F., Felmy, A. R., & Rosso, K. M.: In situ XRD study of Ca2+ saturated montmorillonite (STX-1) exposed to anhydrous and wet supercritical carbon dioxide. International Journal of Greenhouse Gas Control, 6, 220-229, `https://doi.org/10.1016/j.ijggc.2011.11.001`, 2012.

[46] Sciandra, D., Vilarrasa, V., Rahimzadeh Kivi, I., Makhnenko, R., Nussbaum, C., & Rebscher, D.: Coupled HM modeling assists in designing CO2 long-term periodic injection experiment (CO2LPIE) in Mont Terri rock laboratory, In EGU General Assembly Conference Abstracts (pp. EGU21-8982), `https://doi.org/10.5194/egusphere-egu21-8982`, 2021

[47] Stamati, O., Andò, E., Roubin, E., Cailletaud, R., Wiebicke, M., et al.: spam: Software for Practical Analysis of Materials, Journal of Open Source Software, Open Journals, 5 (51), pp.2286, `https://doi.org/10.21105/joss.02286`, 2020.

[48] Stavropoulou, E., Andò, E., Roubin, E., Lenoir, N., Tengattini, A., Briffaut, M., & Bésuelle, P.: Dynamics of water absorption in Callovo-Oxfordian claystone revealed with multimodal x-ray and neutron tomography, Frontiers in Earth Science, 8, 6, `https://doi.org/10.3389/feart.2020.00006`, 2020

[49] Stavropoulou, E., & Laloui, L.: Evaluating CO2 breakthrough in a shaly a caprock material: a multi-scale experimental approach. Scientific Reports, 12(1), 1-19, `https://doi.org/10.1038/s41598-022-14793-8`, 2022.

[50] Vego, I., Tengattini, A., Andò, E., Lenoir, N., & Viggiani, G.: Effect of high relative humidity on a network of a water-sensitive particles (couscous) as revealed by in-situ x-ray tomography, Soft Matter, `https://doi.org/10.1039/D2SM00322H`, 2022.

[51] Viggiani, G., & Hall, S. A.: Full-field measurements, a new tool for laboratory experimental geomechanics, In Proceedings of the 4th Symposium on Deformation Characteristics of Geomaterials, 1, 3-26, 2008.

[52] Viggiani, G., Andò, E., Takano, D., & Santamarina, J. C.: Laboratory X-ray tomography: a valuable experimental tool for revealing processes in soils, Geotechnical Testing Journal, 38(1), 61-71, `https://doi.org/10.1520/GTJ20140060`, 2015.

[53] Vilarrasa, V., Carrera, J., Olivella, S., Rutqvist, J., & Laloui, L.: Induced seismicity in geologic carbon storage, Solid Earth, 10(3), 871-892, `https://doi.org/10.5194/se-10-871-2019`, 2019.

[54] Voltolini, M., & Ajo-Franklin, J. B.: The sealing mechanisms of a fracture in opalinus clay as revealed by in situ synchrotron x-ray micro-tomography, Frontiers in Earth Science, 8, 207, `https://doi.org/10.3389/feart.2020.00207`, 2020.

[55] Wang, L. L., Bornert, M., Chanchole, S., Yang, D. S., Héripré, E., Tanguy, A., & Caldemaison, D.: Micro-scale experimental investigation of the swelling anisotropy of the Callovo-Oxfordian argillaceous rock, Clay Minerals, 48(2), 391-402, `https://doi.org/10.1180/claymin.2013.048.2.17`, 2013.

[56] Wang, S., & Tokunaga, T. K.: Capillary pressure–saturation relations for supercritical CO2 and brine in limestone/dolomite sands: Implications for geologic carbon sequestration in carbonate reservoirs, Environmental science & technology, 49(12), 7208-7217, `https://doi.org/10.1021/acs.est.5b00826`, 2015.

[57] Wollenweber, J., Alles, S., Busch, A., Krooss, B. M., Stanjek, H., & Littke, R.: Experimental investigation of the CO2 sealing efficiency of caprocks, International Journal of Greenhouse Gas Control, 4(2), 231-241, `https://doi.org/10.1016/j.ijggc.2010.01.003`, 2010.

[58] Yang, K., Zhou, J., Xian, X., Zhou, L., Zhang, C., Tian, S., Lu, Z., & Zhang, F.: Chemical-mechanical coupling effects on the permeability of shale subjected to supercritical CO2-water exposure, Energy, 248, 123591, `https://doi.org/10.1016/j.energy.2022.123591`, 2022.

[59] Yasuhara, H., Kinoshita, N., Ohfuji, H., Lee, D. S., Nakashima, S., & Kishida, K.: Temporal alteration of fracture permeability in granite under hydrothermal conditions and its interpretation by coupled chemo-mechanical model, Applied Geochemistry, 26(12), 2074-2088, `https://doi.org/10.1016/j.apgeochem.2011.07.005`, 2021.

[60] Yu, H., Zhang, Y., Lebedev, M., Li, X., Wang, Z., Verrall, M., Squelch, A., & Iglauer, S.: Swelling-induced self-sealing mechanism in fractured caprock: implications for carbon geosequestration. AAPG Bulletin, (20,221,001), `https://doi.org/10.1306/09232219136`, 2022.

[61] Zappone, A., Rinaldi, A. P., Grab, M., Wenning, Q. C., Roques, C., Madonna, C., Obermann, A. C., Bernasconi, S. M., Brennwald, M. S., Kipfer, R., Soom, F., Cook, P., Guglielmi, Y., Nussbaum, C., Giardini, D., Mazzotti, M., & Wiemer, S.: Fault sealing and caprock integrity for CO2 storage: an in situ injection experiment, Solid Earth, 12, 319–343, `https://doi.org/10.5194/se-12-319-2021`, 2021.

[62] Zhang, M., de Jong, S. M., Spiers, C. J., Busch, A., & Wentinck, H. M.: Swelling stress development in confined smectite clays through exposure to CO2. International Journal of Greenhouse Gas Control, 74, 49-61, `https://doi.org/10.1016/j.ijggc.2018.04.014`, 2018.